Natural Resources Canada | Ressources naturelles Canada

GEOLOGICAL SURVEY OF CANADA
OPEN FILE 7661

Atlas of Sonobuoy Velocity Analyses in Canada Basin

D. Chian and N. Lebedeva-Ivanova

2015

Canada

GEOLOGICAL SURVEY OF CANADA
OPEN FILE 7661

Atlas of Sonobuoy Velocity Analyses in Canada Basin

D. Chian[1] and N. Lebedeva-Ivanova[2]

[1] Chian Consulting, 6238 Regina Terr., Dartmouth, Nova Scotia
[2] Woods Hole Oceanographic Institution, Woods Hole, MA
Current Address: University of Oslo, Oslo, Norway

2015

doi:10.4095/295857

This publication is available for free download through GEOSCAN (http://geoscan.nrcan.gc.ca/).

Recommended citation
Chian, D. and Lebedeva-Ivanova, N., 2015. Atlas of Sonobuoy Velocity Analyses in Canada Basin; Geological Survey of Canada, Open File 7661, 1 zip file. doi:10.4095/295857

Publications in this series have not been edited; they are released as submitted by the author.

Atlas of Sonobuoy Velocity Analyses in Canada Basin

Authors: Deping Chian[1] and Nina Lebedeva-Ivanova[2]

[1] Chian Consulting, Dartmouth, Nova Scotia (deping.chian@gmail.com)
[2] Woods Hole Oceanographic Institution, Woods Hole, MA
Current Address: University of Oslo, Oslo, Norway

Suggested Citation:
Chian, D., and Lebedeva-Ivanova, N., 2015, Atlas of Sonobuoy Velocity Analyses in Canada Basin; Geological Survey of Canada Open File 7661, 1 zip file. doi:10.4095/295857

Table of Contents

1 Abstract

Canada Basin of the Arctic Ocean is located in one of the most remote, ice-covered regions on Earth. This Atlas presents the data and velocity models for 144 out of 174 sonobuoys launched throughout and north of the Canada Basin between 2007 and 2011. The data, which are coincident with multichannel seismic reflection profiles, were acquired to map p-wave velocities and thicknesses of the sedimentary column. The refraction and wide-angle reflection data provide the basis for transformation of seismic reflection travel time data to the depth domain. Two independent approaches were utilized to obtain velocity models from the sonobuoy data: forward modeling (FM) of refracted arrivals and semblance analysis (SA) of wide-angle reflections. Sonobuoys with both FM and SA number 99. Agreement between the data sets is excellent. The maximum difference between the methods is about 10% and more than half of the measurements agree to within 5%. This atlas is a first release of these data with preliminary analyses and interpretations.

2 Introduction

The Canada Basin of the Arctic Ocean is one of the most remote, ice-covered regions on Earth. Between 2007 and 2011, more than170 sonobuoys were launched throughout and north of the Canada Basin in concert with a seismic reflection program to map sedimentary p-wave velocities and thicknesses (Figure 1; Table 1). The refraction and wide-angle reflection data provide the basis for transformation of seismic reflection travel time data to the depth domain. The program proved to be a technological and scientific success because of the high quality of data acquired, with refractions observed sometimes well into basement rocks and occasionally from the upper mantle.

The sonobuoy program was part of a joint Canadian and U.S. program to map the Extended Continental Shelf under Article 76 of the United Nations Convention on the Law of the Sea, for which mapping sediment thickness is a vital component. The sonobuoy system was operated from *CCGS Louis S. St-Laurent*. For 2008-2011, the data were collected during two-icebreaker expeditions in which *USCGC Healy* broke ice ahead of *CCGS Louis S. St-Laurent*. In 2007, the data were acquired from *CCGS Louis S. St-Laurent* without the aid of a second icebreaker.

Two independent approaches were utilized to obtain velocity models from the sonobuoy data: forward modeling (FM) of refracted arrivals and semblance analysis (SA) of wide-angle reflections. Each of these techniques utilizes different types of information acquired by the sonobuoys. The FM method typically includes interpretations for the full extent of the data (i.e., to offsets of 25-40 km) and models the diving (refracted) waves. The SA method utilizes the wide-angle reflections that are limited to offsets of 7 km and therefore represent primarily sedimentary reflections. Each technique represents the work of two independent researchers using two independent software packages (Chian for FM utilizing SeisWide software, Lebedeva-Ivanova for SA utilizing ProMAX® commercial software). Consequently, the interpretations for each technique have high internal consistency. In combining the results in this Atlas, the remarkably high consistency between methods is also shown.

The purpose of this Atlas is to release these sonobuoy data and analyses including a comparison of the FM and SA results. The comparison focuses on depths where the analyses overlap, i.e., within the sedimentary column. This report also summarizes information about the airgun source, the sonobuoy hydrophone receiver, the coincident multichannel seismic reflection data, the methodology used in FM, and the methodology used in SA. The final section presents a brief comparison of the two data sets for the sedimentary section.

Tables of all FM velocity data are presented in Appendix I. Tables of all SA data are presented in Appendix II. While many details of data acquisition are presented in this Atlas, additional instrument diagrams, field configurations, and parameters are given in expedition cruise reports (Mosher et al., 2009, Jackson and DesRoches, 2010, Mosher et al., 2010, Mosher, 2012).

2.1 Using this Atlas

The data and results for each sonobuoy are presented on three pages:

Page 1 shows the raw and processed sonobuoy data together with the uninterpreted multichannel reflection profile. The upper panel shows the raw sonobuoy data; the middle panels show the same data processed for FM and SA. The lower panel displays the portion of the multichannel data

coincident with the sonobuoy. These plots were generated with SeisWide software and assembled in CorelDraw.

Page 2 shows the sonobuoy data and interpretations from FM analysis. The upper panel shows the sonobuoy data together with modeled refracted and wide-angle arrivals of the best-fit velocity solution, commonly with an inset showing the modeling of shallow refraction phases . The middle panel shows the velocity model and associated raypaths superimposed on depth-converted multichannel data. The lower panel shows the velocity model superimposed on the coincident multichannel data in two-way travel-time (TWTT) domain, with optionally a velocity-depth curve at the sonobuoy location. These plots were generated with SeisWide software and assembled in CorelDraw. Modeled P-wave refractions from layer i are labeled as Pi in red, while modeled wide-angle reflections are marked Ri in blue. In rare cases S-wave refractions are well defined and modeled (e.g. 2009-12-1, 2009-13-1, 2009-13-2, 2009-18-1, 2009-19-1, 2011-01, and 2011-05). S-refractions (Si) are all converted at the ~4.5km/s layer at shallow depths, above which they travel as P-waves and below which as S-waves and refracts at i-th layer (see central panels for their raypaths in blue). S-wave velocities are labeled with brackets; σ represents Poisson's ratio.

Page 3 shows the sonobuoy data interpreted for SA (upper) and plots/tables of the modeling and semblance results combined (lower). The semblance panels show, from the left, the coincident multichannel data, the coherency plot with velocity picks, the processed sonobuoy record to 7 km, and the normal-moveout-corrected (and muted) sonobuoy record for the velocity picks. The red circle in the coherency plot is the depth of the last reliable pick. The lower panel compares the interval and rms velocities of both methods versus two-way travel time in the left plot, both time-depth functions in the right plot, and tables of relevant times, depths, and velocities for both methods. Page 3 plots were generated using ProMAX® software (upper) or Matlab (lower) and assembled using Adobe Illustrator.

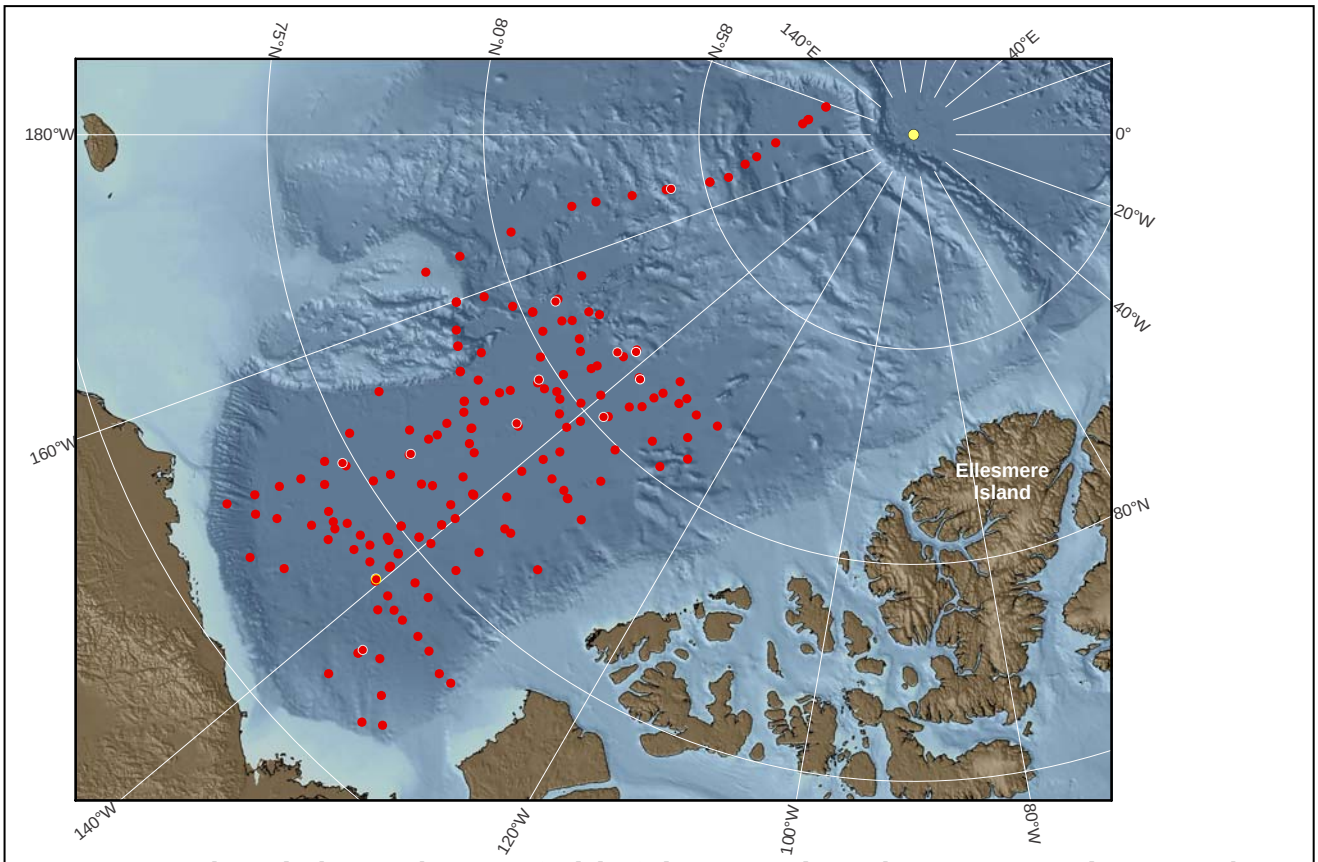

Figure 1: Sonobuoy deployment locations (red dots) during expeditions between 2007 and 2011. North pole is marked by yellow circle. Stereographic projection with standard parallel at 75^0.

Table 1: Sonobuoy deployment locations and line end points

SB	LON_START	LAT_START	LON_END	LAT_END	LON_DROP	LAT_DROP	DEPTH (m)	FM	SA
2007							*2007 subtotal*	*23*	*20*
2007-01	-138.268356	74.480736	-138.009308	74.510452	-138.04801	74.474650	30		X
2007-02	-143.891357	76.187859	-143.258102	76.224556	-143.893804	76.187505	30	X	
2007-03	-140.097137	76.128136	-139.522736	76.087341	-140.067134	76.129385	30	X	X
2007-04	-130.149475	73.385719	-130.925644	73.432739	-130.146242	73.385577	30	X	
2007-05	-131.364426	73.352959	-132.038620	73.344025	-131.339587	73.379300	30	X	
2007-06	-133.174286	73.606430	-133.856979	73.753845	-133.172004	73.605869	60	X	
2007-08	-134.671219	73.668655	-135.518311	73.700623	-134.670396	73.668588	60	X	
2007-09	-137.349444	73.697194	-138.419939	73.834383	-137.525872	73.690081	60	X	
2007-10	-138.757163	73.805594	-139.880897	73.844528	-138.756772	73.805446	60	X	X
2007-11	-140.482939	73.851499	-141.606315	73.930632	-140.479538	73.851010	60	X	X
2007-12	-141.862027	73.983463	-142.960136	73.868774	-141.860119	73.982893	60	X	X
2007-13	-143.463957	73.868044	-144.508652	73.867943	-143.462066	73.867828	60	X	X
2007-15	-146.310719	73.853929	-147.435109	73.844679	-146.306332	73.853828	60	X	X
2007-16	-147.614166	76.146774	-147.602707	76.177208	-147.615007	76.144920	60		X
2007-17	-147.613439	76.192483	-147.736136	76.487942	-147.61075	76.188718	60	X	X
2007-18	-147.886581	76.707901	-148.612370	76.962526	-147.883309	76.707363	60	X	X
2007-19	-148.206619	77.196854	-147.959854	77.15345	-148.207522	77.197038	60		X
2007-20	-147.000124	75.540700	-146.996995	75.246189	-146.999936	75.548539	60	X	X
2007-21	-147.351837	75.124242	-148.278934	74.993665	-147.339377	75.126053	60	X	X
2007-22	-149.734312	74.774912	-150.820070	74.604393	-149.735164	74.774775	60	X	X
2007-23	-150.996422	74.391815	-150.053099	74.240894	-150.999181	74.392527	60	X	X
2007-24	-149.315338	74.134964	-148.339157	73.979431	-149.316648	74.135182	60	X	X
2007-25	-147.212134	73.883571	-146.149009	74.015352	-147.21632	73.883291	60	X	X
2007-26	-145.553861	74.086875	-144.456958	74.169948	-145.555296	74.086755	60	X	X
2007-27	-144.103760	74.181503	-143.015259	74.204414	-144.104508	74.181431	60	X	X
2007-28	-142.953757	74.220214	-142.558514	74.505049	-142.953927	74.220161	60	X	X
2008							*2008 subtotal*	*30*	*28*
2008-01	-140.320182	73.809355	-140.433770	74.099725	-140.319495	73.808171	60	X	X
2008-02	-140.485394	74.259300	-140.592643	74.553751	-140.485210	74.285770	60	X	X
2008-03	-140.901436	74.610943	-142.123762	74.627636	-140.899360	74.610930	60	X	X
2008-04	-142.605208	74.651294	-142.715080	74.973186	-142.604975	74.650964	60	X	X
2008-05	-142.618545	75.054258	-141.465673	75.162504	-142.620170	75.054070	60	X	X
2008-06	-140.827232	75.221014	-139.646780	75.311872	-140.84388	75.219420	60	X	X
2008-07	-139.728597	75.334649	-140.177704	75.642810	-139.72811	75.334370	60	X	X
2008-08	-140.422260	75.805170	-140.992626	76.089754	-140.42137	75.804583	60	X	X
2008-10	-142.802770	76.875437	-143.321153	77.163484	-142.80268	76.874240	60	X	X
2008-12	-146.508645	77.678671	-147.860164	77.770708	-146.42764	77.685160	60	X	X
2008-13	-149.333204	77.872778	-150.759983	77.978312	-149.33321	77.872800	60	X	X
2008-15	-155.119553	78.337051	-156.521576	78.416092	-155.118714	78.337003	60	X	
2008-18	-159.327972	79.343697	-158.214196	79.601381	-159.34493	79.338470	60	X	X
2008-19	-156.823310	79.864665	-155.562091	80.105131	-156.83361	79.862431	60	X	X
2008-21	-152.119530	80.752283	-151.598187	80.992240	-152.12368	80.751590	60	X	

SB	LON_START	LAT_START	LON_END	LAT_END	LON_DROP	LAT_DROP	DEPTH (m)	FM	SA
2008-22	-142.094673	81.848281	-140.128660	81.678030	-142.094673	81.848281	60	X	X
2008-23	-138.413541	81.474445	-136.521450	81.320170	-138.413541	81.474445	60	X	X
2008-24	-134.972321	81.065273	-133.242705	80.897780	-134.972321	81.065273	60	X	X
2008-25	-131.967702	80.724785	-130.108140	80.607490	-131.967702	80.724785	60	X	X
2008-28	-133.408565	79.909827	-134.535163	79.827835	-133.407974	79.910059	60	X	X
2008-29	-139.303028	79.781137	-140.902711	79.752919	-139.292137	79.791544	60	X	X
2008-30	-143.234279	79.735128	-144.363099	79.672919	-143.232531	79.735224	60	X	X
2008-31	-147.118774	79.573799	-145.473068	79.580910	-147.118583	79.573838	60	X	X
2008-32	-141.733227	79.521792	-140.030944	79.479594	-141.739038	79.521982	60	X	X
2008-34	-130.801585	78.193964	-132.295228	78.305095	-130.797350	78.193417	60	X	X
2008-35	-133.598236	78.345947	-134.373352	78.387321	-133.583471	78.344956	60	X	X
2008-36	-134.514176	78.419912	-136.204795	78.460652	-134.506596	78.419636	60	X	X
2008-37	-138.757950	78.564514	-139.782928	78.680061	-138.756819	78.564452	60	X	X
2008-38	-143.609844	78.593755	-142.293781	78.424900	-143.613460	78.593533	60	X	X
2008-39	-139.334455	78.004746	-137.990615	77.863002	-139.335621	78.004967	60	X	X
2009							*2009 subtotal*	*44*	*41*
2009-01-1	-148.267161	77.261900	-148.342485	77.570334	-148.268178	77.260971	60	X	X
2009-01-2	-148.336923	77.735077	-148.258784	78.067308	-148.337132	77.735059	60	X	X
2009-01-3	-148.164171	78.270846	-147.908239	78.603531	-148.164437	78.270733	60	X	X
2009-01-4	-147.609264	78.909978	-147.198991	79.205972	-147.610036	78.909285	60	X	X
2009-01-5	-146.573698	79.535336	-145.970581	79.842089	-146.574686	79.534729	60	X	X
2009-01-6	-145.597073	80.140927	-144.992604	80.451434	-145.599039	80.140265	60	X	X
2009-02-1	-144.056352	80.739370	-142.236635	80.647922	-144.057782	80.739501	60	X	X
2009-02-2	-140.195465	80.544219	-138.451121	80.446367	-140.227307	80.544025	60	X	X
2009-03-1	-137.256840	80.342189	-138.910363	80.228511	-137.254414	80.342291	60	X	X
2009-03-2	-141.092697	80.063862	-142.701225	79.927845	-141.091365	80.063883	60	X	X
2009-03-3	-144.284283	79.783401	-145.755138	79.638835	-144.282290	79.783596	60	X	X
2009-04-1	-146.818802	79.592522	-148.154495	79.774315	-146.819980	79.592629	60	X	X
2009-04-2	-149.210350	79.909074	-150.706052	80.094055	-149.209498	79.908941	60	X	X
2009-04-3	-152.075190	80.246694	-153.696071	80.441393	-152.062868	80.245449	60	X	X
2009-04-4	-155.017993	80.820337	-155.015674	80.923187	-155.016955	80.819929	60	X	X
2009-05-1	-155.240107	80.896782	-155.988969	81.202626	-155.226728	80.892271	60	X	X
2009-06-1	-156.997330	81.618866	-155.034387	81.549496	-157.000721	81.618965	60	X	X
2009-07-1	-151.375065	81.401699	-150.105542	81.588327	-151.405012	81.397118	60	X	X
2009-08-1	-150.197168	81.583935	-151.000261	81.293900	-150.194289	81.584798	60	X	
2009-10-1	-151.421492	80.961987	-149.474112	80.920477	-151.423499	80.962058	60	X	X
2009-11-1	-148.599472	80.895432	-147.482208	80.862503	-148.603132	80.895601	60		X
2009-12-1	-146.880360	80.763470	-144.899419	80.746120	-146.947057	80.765323	60	X	X
2009-13-1	-143.871116	80.895321	-143.191833	81.219839	-143.811097	80.895083	60	X	X
2009-13-2	-142.603183	81.509880	-141.872643	81.791761	-142.604174	81.509600	60	X	
2009-14-1	-141.973586	81.804361	-144.166509	81.839556	-141.970498	81.807048	60	X	X
2009-18-1	-143.712883	81.452320	-141.745770	81.462832	-143.719910	81.452310	60	X	X
2009-19-1	-138.147635	81.465551	-136.209824	81.535329	-138.196805	81.463695	60	X	X
2009-21-1	-134.087848	81.633104	-132.229226	81.788334	-134.093038	81.632519	60	X	X
2009-21-2	-130.638423	81.908737	-128.550814	82.049716	-130.639110	81.908746	60	X	X

SB	LON_START	LAT_START	LON_END	LAT_END	LON_DROP	LAT_DROP	DEPTH (m)	FM	SA
2009-23-1	-123.959956	81.828734	-126.207290	81.810423	-123.958758	81.828761	60	X	X
2009-24-1	-131.158265	81.704027	-132.993356	81.547599	-131.154033	81.704357	60	X	X
2009-25-1	-134.639558	81.392381	-135.529998	81.117232	-134.585481	81.400571	60	X	
2009-25-2	-136.224209	80.869017	-136.949099	80.576675	-136.223366	80.844146	60	X	X
2009-25-3	-137.702572	80.255190	-138.336463	79.963372	-137.701454	80.256145	60	X	X
2009-26-1	-139.829557	79.455445	-138.927599	79.203544	-139.829727	79.455567	60	X	X
2009-26-2	-138.104359	78.961707	-137.291391	78.710146	-138.105579	78.962114	60	X	X
2009-28-1	-136.406829	78.409473	-136.629463	78.107695	-136.406589	78.409551	60	X	X
2009-30-1	-138.294357	77.350426	-137.222870	77.131134	-138.294571	77.350527	60	X	X
2009-31-1	-135.316803	76.846809	-136.700607	76.862396	-135.312019	76.846836	60	X	X
2009-31-2	-137.871140	76.860611	-139.063538	76.856270	-137.870522	76.860583	60	X	X
2009-32-2	-147.806763	76.931602	-149.127365	76.952065	-147.796674	76.931334	60	X	
2009-33-1	-153.271500	78.754471	-151.624893	78.750839	-153.272660	78.754497	60	X	X
2009-34-1	-144.007979	78.601919	-144.425340	78.320652	-144.007406	78.602150	60	X	X
2009-35-1	-145.203045	77.445066	-145.619847	77.144712	-145.202699	77.445167	60	X	X
2009-36-1	-144.650232	76.000293	-144.155025	75.713078	-144.651515	76.001067	60	X	X
2010							*2010 subtotal*	*33*	*15*
2010-01	-147.446824	71.818977	-146.686948	71.989353	-147.444102	71.819578	60	X	
2010-02	-145.408304	72.320466	-145.383327	72.657876	-145.408412	72.319458	60	X	X
2010-03	-145.329493	73.520406	-145.308134	73.832379	-145.329580	73.518955	300	X	X
2010-04	-145.738289	73.785364	-146.473317	73.560366	-145.747750	73.782415	30	X	X
2010-05	-147.035613	73.388504	-147.719893	73.173877	-147.030417	73.390105	60	X	X
2010-06	-148.903948	72.799052	-149.595224	72.574258	-148.902575	72.799477	60	X	
2010-07	-150.040343	72.429068	-150.712806	72.208130	-150.038002	72.429790	60	X	
2010-08	-151.743075	71.979241	-151.558585	72.285060	-151.743550	71.978230	60	X	
2010-09	-151.354283	72.635096	-151.175633	72.934018	-151.354288	72.635337	60	X	
2010-10	-150.962426	73.280773	-150.808536	73.533985	-151.003102	73.211170	60	X	
2010-11	-150.689537	73.722600	-150.445239	74.035381	-150.690410	73.721623	60	X	
2010-12	-150.128587	74.739253	-151.122520	74.955973	-150.127582	74.738998	60	X	X
2010-13	-152.121285	75.210358	-153.143121	75.389917	-152.119855	75.210105	60	X	X
2010-14	-153.051875	76.294636	-154.351434	76.237445	-154.307117	76.239508	60	X	X
2010-15	-149.632643	76.449860	-148.262512	76.508423	-149.631070	76.449955	60	X	X
2010-16	-150.638764	78.390751	-149.195926	78.549778	-150.638157	78.390855	60	X	X
2010-17	-148.080631	78.672460	-146.677797	78.824765	-148.082093	78.672330	60	X	X
2010-18	-133.344342	82.097398	-131.180493	81.948787	-133.373270	82.100595	60	X	X
2010-19	-127.743568	81.753296	-127.053078	81.730194	-127.746353	81.753501	60		X
2010-20	-130.787501	76.660535	-132.156665	76.723822	-130.822870	76.662382	60	X	
2010-21	-136.031978	76.820552	-136.080493	76.512864	-136.031860	76.820600	60	X	X
2010-22	-136.147032	76.019150	-136.209535	75.692095	-136.146888	76.019033	60	X	X
2010-23	-136.395125	75.345547	-136.425679	75.028093	-136.395137	75.345892	60	X	
2010-24	-136.371657	74.458012	-136.456571	74.170612	-136.371502	74.458082	60	X	
2010-25	-136.498414	73.676666	-136.711014	73.288010	-136.498303	73.676757	60	X	
2010-26	-136.983153	72.431771	-136.643609	72.928968	-136.983458	72.431108	60	X	
2010-27	-136.993177	72.418439	-137.061781	72.119660	-136.992288	72.419355	60	X	
2010-28	-137.341030	71.608538	-137.514374	71.247002	-137.340935	71.608438	60	X	

SB	LON_START	LAT_START	LON_END	LAT_END	LON_DROP	LAT_DROP	DEPTH (m)	FM	SA
2010-29	-133.899429	71.321503	-132.761948	71.410660	-133.187700	71.37800	60	X	
2010-30	-131.955402	71.643228	-132.611356	71.847314	-131.955635	71.643248	60	X	
2010-31	-134.886298	72.513596	-133.473012	72.111137	-133.514328	72.122707	60	X	
2010-32	-135.532229	72.694371	-136.455978	72.935356	-135.532050	72.694272	60	X	
2010-33	-139.189762	73.588259	-137.705681	73.258733	-138.438307	73.423583	60	X	
2010-34	-140.395622	73.846633	-141.483908	73.771971	-140.396282	73.846552	60	X	X
2011							*2011 subtotal*	*10*	*0*
2011-01	-164.299097	78.230556	-164.555571	78.547592	-164.295455	78.226195	60	X	
2011-02	-165.025824	79.060330	-165.254007	79.306976	-165.016217	79.084383	60	X	
2011-03	-166.445524	80.392149	-166.808729	80.684559	-166.425908	80.375172	60	X	
2011-04	-168.237143	81.875982	-168.167014	82.196143	-168.238017	81.875360	60	X	
2011-05	-168.099919	82.452947	-168.004876	82.769145	-168.100183	82.452876	60	X	
2011-06	-167.840878	83.307531	-167.764027	83.553622	-167.850617	83.303833	60	X	
2011-08	-167.494954	84.221395	-167.343459	84.531849	-167.501930	84.213190	60	X	
2011-09	-167.011604	85.126681	-167.192671	84.831032	-166.977333	85.134000	60		
2011-10	-167.010917	85.134028	-166.813840	85.447191	-167.011347	85.134126	60		
2011-11	-167.077358	85.580414	-168.784602	85.866324	-167.073423	85.579687	60		
2011-12	-170.118575	86.019861	-172.015505	86.303266	-170.155473	86.020188	60		
2011-14	-176.665203	86.788316	-179.997581	87.053887	-176.673660	86.788964	60		
2011-15	174.161650	87.410238	171.924802	87.512267	174.161650	87.410238	60		
2011-16	171.173839	87.545808	165.861604	87.747746	171.473506	87.532715	60		
2011-17	162.131228	87.863122	154.869998	88.026875	162.120513	87.863534	60		
2011-19	-126.691284	81.198950	-125.745939	80.925612	-126.711611	81.208876	60	X	
2011-20	-124.892494	80.812355	-123.931511	80.696754	-124.888348	80.811852	60	X	
2011-21	-127.390550	80.255687	-128.634328	80.402843	-127.374814	80.292694	60	X	
							TOTAL	***138***	***104***

3 Airgun Seismic Source

Seismic refraction data were acquired with an airgun seismic sound source deployed from the vessel CCGS *Louis S. St-Laurent.* Although the data were acquired over five field programs (2007-2011), the acquisition parameters did not vary significantly from season to season.

The seismic source was an 1150 in^3 pneumatically charged array (Figure 2) of three Sercel G-guns: 2 x 500 in^3 and 1 x 150 in^3 in size. This source was chosen for its compact size, peak power, and frequency spectrum of the emitted pulse (~2-60 Hz). Repeatability of the source signature was achieved through synchronizing firing of the three guns to within 1 millisecond. Two airgun arrays were available for redundancy. The array was towed at 11.5 to 12 m water depth immediately astern of the vessel utilizing a 3500-lb hydrodynamic depressor weight to keep the array near the stern of the vessel and protected from the ice.

The seismic source was activated between 17 and 20 second intervals, depending on water depth, while the ship proceeded at a nominal speed of 4 knots. Because of ice conditions and ice breaking, speed varied substantially, thus there is significant variability in shot spacing.

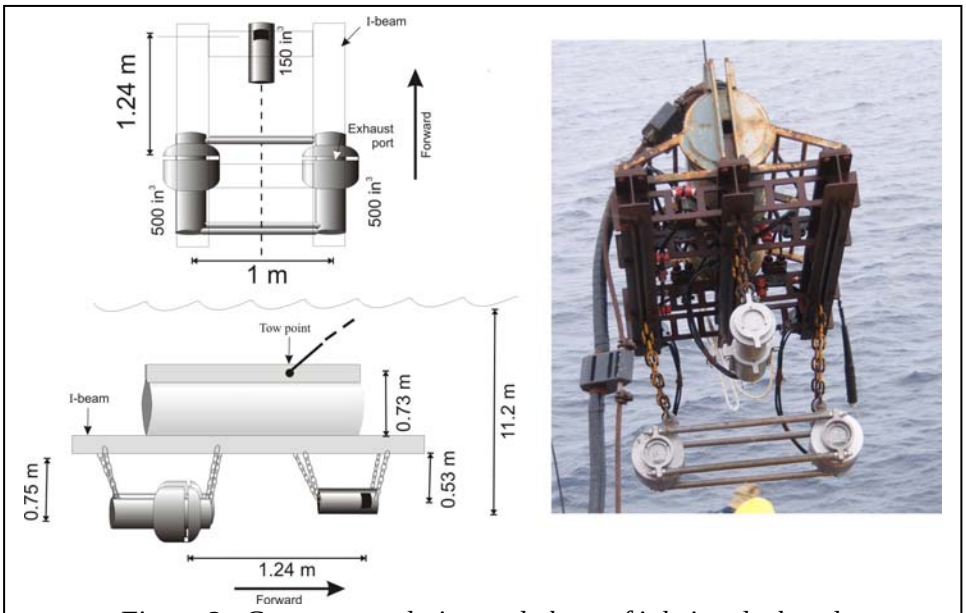

Figure 2. G-gun array design and photo of it being deployed.

During the 2009 and 2010 field programs, source calibration and amplitude decay experiments were conducted. The measured signal strength of the 1150 in^3 array at 0-to-peak amplitude was 5.29 Bar-m, or ~235 dB re 1 µPa at 1 m (Figure 4-2 in Appendix 4). The amplitude decay with distance was found to follow a spherical spreading pattern only for distances up to 500 m (i.e., follow a 20Log(R) curve where R is the radius of the sphere of the wavefront) (see Appendix 3). Amplitude decay beyond 500 m was greater than predicted for spherical spreading. While this discrepancy remains unexplained, it is most likely caused by the complex water column velocity structure in the polar ocean, especially the uppermost 200 m below the ice where low velocity zones can occur. Friction and other attenuation losses are not considered either. Both of these experiments and additional description are given in respective cruise reports of 2009 and 2010 (Mosher et al., 2009; Mosher et al., 2010) and are summarized in Appendix 4.

4 Expendable Sonobuoy Receivers

Free-floating Ultra-Electronics marine sonobuoys (Model 53C; see top of Figure 3) were deployed to acquire wide angle reflection and refraction data for velocity determination. The sonobuoys lack an internal navigation system and, following deployment, are assumed to move with currents or, in the case of the Arctic deployments, with ice movement. The bottom of Figure 3 shows an estimation of the drift of the ice behind the vessel. Since the ice movements are not in the same line with our seismic experiment, actual sonobuoy drift are estimated to be greater than the inline sonobuoy drift, but less than twice of that amount. From the 10 sample sonobuoy statistics in Figure 3, inline drifts during the first 4 hours of operation are mostly 0-1.5 km. In the cases of a flat layer structure, of which the majority of Canada Basin is characterized on a 30-km scale, such sonobuoy drifting has no effect on the model results. But when there are out of the plane structural changes, sonobuoy drifting starts to have effects which will need to be taken into account during the modeling process.

The majority of sonobuoys were vertically dropped into the sea from the ship's stern rail, at irregular but frequent intervals, particularly over straight-line segments meant to be greater than 35 km in length. For a few deployments, the sonobuoys were launched from a helicopter in advance of the ship in order to acquire pseudo-reversed profiles. In these instances, only a single sonobuoy could be recorded at one time, so the forward sonobuoy was recorded until the ship was abreast of the buoy,

then a second sonobuoy was deployed from the stern to record data as the ship was moving away. Hence these pseudo-reversed lines record data in opposite directions, though only over adjacent segments of a survey line. For all but some testing deployments, the sonobuoy hydrophone was activated at 60 m water depth (table 1). The sonobuoys auto-scuttled after 8 hours of operation.

4.1 Telemetry

Sonobuoy-received seismic signals were radio-telemetered (VHF) to sonobuoy receivers mounted on the ship's crow's nest structure. In 2007 and 2008, an omnidirectional antenna was used. In 2009 – 2011, a stacked array of two antennas, cut to respond to frequencies between 150 and 160 MHz were fitted to the aft railing, port side of the "crow's nest". This array has a 15º beam width pattern focussed astern of the vessel and significantly improved signal to noise ratios of the sonobuoy data compared to the omnidirectional configuration. A similar array was fitted to look forward of the vessel for sonobuoys that were deployed by helicopter ahead of the ship. A high pass RF filter prevented damage to the sonobuoy receivers from the strong signal of the helicopter DF beacon. Signal reception on the beam focused array was excellent, often received up to 35 km distance and beyond. RF interference sometimes significantly affected sonobuoy data quality in the first two years of sonobuoy acquisition, but coordination between sonobuoy and helicopter operations minimized these disturbances in subsequent years. In addition, periodic bursts of noise of unknown source but within seismic frequencies appear on some of the records.

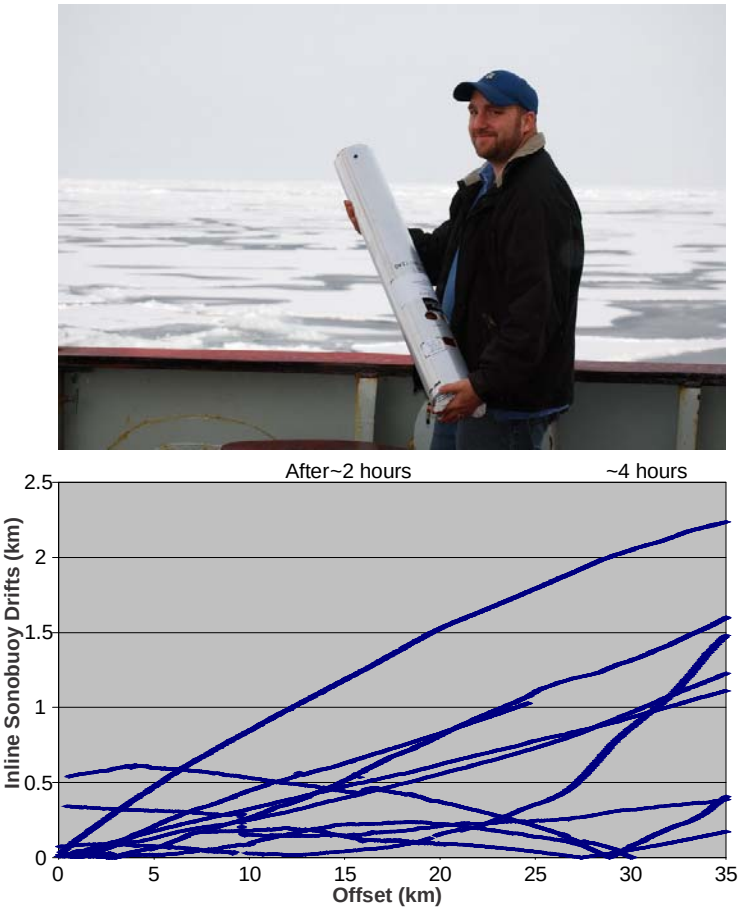

Figure 3. Top: Sonobuoy being deployed off the quarter deck of the CCGS Louis S. St-Laurent. Bottom: Inline sonobuoy drift distance versus computed offset for 10 sample sonobuoys (randomly chosen). Inline sonobuoy drift distance is defined as the absolute difference between computed offset and the fixed offset of the sonobuoy drop location.

4.2 Data Acquisition

Analog data from the telemetry receiver were input to a Geological Survey of Canada digital data logger (GSCDig #4) and digitized by a 24 bit analog-to-digital card, then logged to hard drive. Typical digitizing windows were 18-20 seconds with the window length set to slightly shorter than the airgun firing period. The seismic trigger pulse from the clock was supplied to the digitizer to initiate recording. Maximum sample rate was typically about 290 Hz. Navigation data were recorded as part of the SEG-Y header file and give the ship's navigation antenna location at the time of the shot.

4.3 Summary Statistics

Sonobuoy performance through the five field experiments was excellent, with 89 % success rate recording useable data, i.e., containing coherent arrivals at offsets up to or exceeding 7 km, i.e., useable for SA. Of the total sonobuoys recording useful data (154), about 90 %, or 138 sonobuoys, recorded data to far ranges suitable for FM of the refraction arrivals. SA was only performed for sonobuoys deployed in 2007-2010, and is ~76 % (104) of the total sonobuoys with useable data for those years (136). Seven sonobuoys malfunctioned early in the recording, but still recorded sufficient traces for SA. Table 2 summarizes the number of sonobuoy deployments and their usage.

Table 2. Summary Statistics about sonobuoy deployments and usage (compiled pages for each year are clickable).

Year	Total Sonobuoys Deployed	Total Sonobuoys with useable data (Page 1)	Total sonobuoys used in FM (Page 2)	Total sonobuoys used in SA (Page 3)	Sonobuoys with no useful data	Total sonobuoys used for this atlas.	Sonobuoys with both Pages 2 and 3
2007	28	26	23	20	2	26	17
2008	39	32*	29	28	7	30*	28
2009	52	45	44	41	7	45	40
2010	34	33	33	15	1	33	14
2011	21	18**	10	0	3	10**	0
Totals	174	154	138	104	20	144	99

* 2 sonobuoys recorded good signal-to-noise data for the full 8 hours of recording, but were in regions of large basement relief and were therefore not modeled.

** 9 sonobuoys from the Alpha Ridge and Makarov Basin were of generally good quality but were not analyzed for this study.

5 Shot-Sonobuoy Offset Determination

Because sonobuoys lack location systems, one of the most important initial steps in processing the sonobuoy data is to determine source-to-sonobuoy offset using the arrival time of the direct wave in the water. The offset can be estimated by measuring or assuming a water velocity and accurately measuring the time-break of the water arrival, which is often the highest amplitude arrival on the data record. Developing an empirical function for the relationship between water velocity and travel times provides an efficient means of estimating offsets for a large sonobuoy dataset. The resulting geometry of the data is assumed to be two dimensional.

5.1 Canada Basin Water Velocity

In many previous studies, a constant velocity of seismic wave propagation has been assumed and used for offset calculations. However, the water-velocity profile measured during the 2009 seismic calibration (Figure 4-5, Appendix 4), in the Arctic in general (Figure 4-6 of Appendix 4; Kutschale, 1969, Gavrilov and Mikhalevsky, 2002), and in the oceans in general, is not constant due to variations in salinity, temperature and pressure with depth.

In order to develop a model of the water velocity, a number of CTD from the 2009 field program (Mosher et al., 2009) were used to derive an empirical function with the following criteria: (a) a smooth variation of misfit with the model; and (b) minimum misfit at offsets of 0-7 km. This approach assumes two dimensionality of the geometry, which is satisfied by assumed low drift of ice during the 8-hour deployment window. Figure 4 illustrates both the raypaths in the water and modeled arrivals of the direct water wave for different velocity functions.

The derived equation for determining offsets based on the water velocity is:

$X\ (Tw) = 1.441*Tw+0.00075*Tw^2-0.006,$

where X is offset in kilometres and Tw is direct-wave arrival time in seconds (Lebedeva-Ivanova & Lizarralde, 2011). The derived empirical function is for a receiver depth at 60 m.

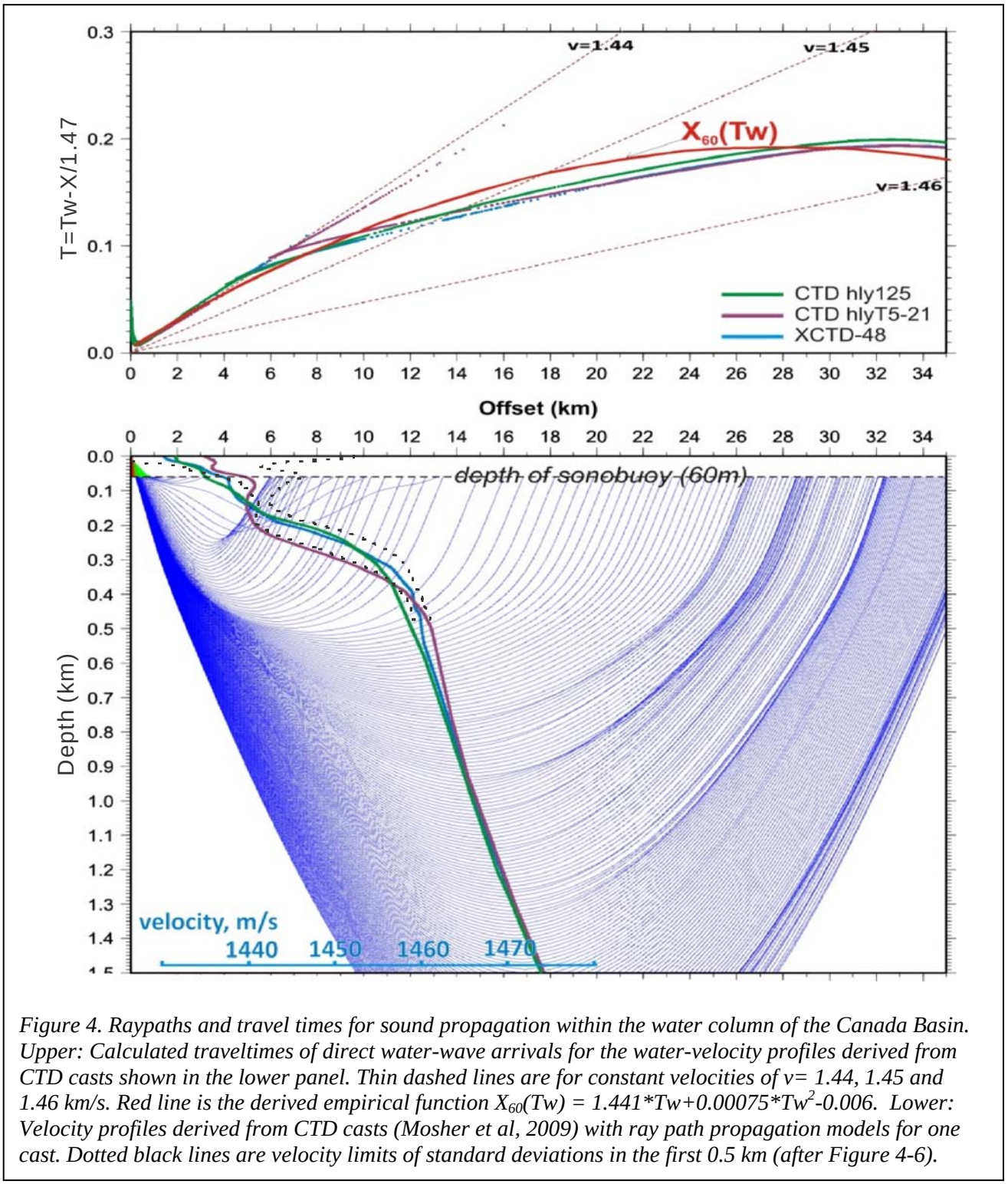

Figure 4. Raypaths and travel times for sound propagation within the water column of the Canada Basin. Upper: Calculated traveltimes of direct water-wave arrivals for the water-velocity profiles derived from CTD casts shown in the lower panel. Thin dashed lines are for constant velocities of v= 1.44, 1.45 and 1.46 km/s. Red line is the derived empirical function $X_{60}(Tw) = 1.441*Tw+0.00075*Tw^2-0.006$. Lower: Velocity profiles derived from CTD casts (Mosher et al, 2009) with ray path propagation models for one cast. Dotted black lines are velocity limits of standard deviations in the first 0.5 km (after Figure 4-6).

The above formula does not converge and therefore gives a negative value when Tw=0, which is an invalid value. For simplicity, at offsets of less than 1 km, the traditional linear raypath formula with V = 1.441 km/s for assigning the offsets is used. In actuality, many of the traces between zero and 1 km offset were unusable because of oversaturation of the signal during recording.

The difference in offset estimates between a constant velocity assumption and an empirical function can be quite large at large offsets (Figure 4). For offsets greater than 15 km, the estimated error is reduced from ~500 m for assumptions of constant velocity to ~ 25 m for the given empirical function. For offsets less than 7 km, error estimates are not more than ~10 m (Figure 5). Hence, the empirical function substantially improves offset estimates by an order of magnitude. If the hydrophone depth is 120 m, the derived function yields errors of up to ~15 m for offsets of ~7 km and up to ~40 m at longer offsets (Lebedeva-Ivanova & Lizarralde, 2011).

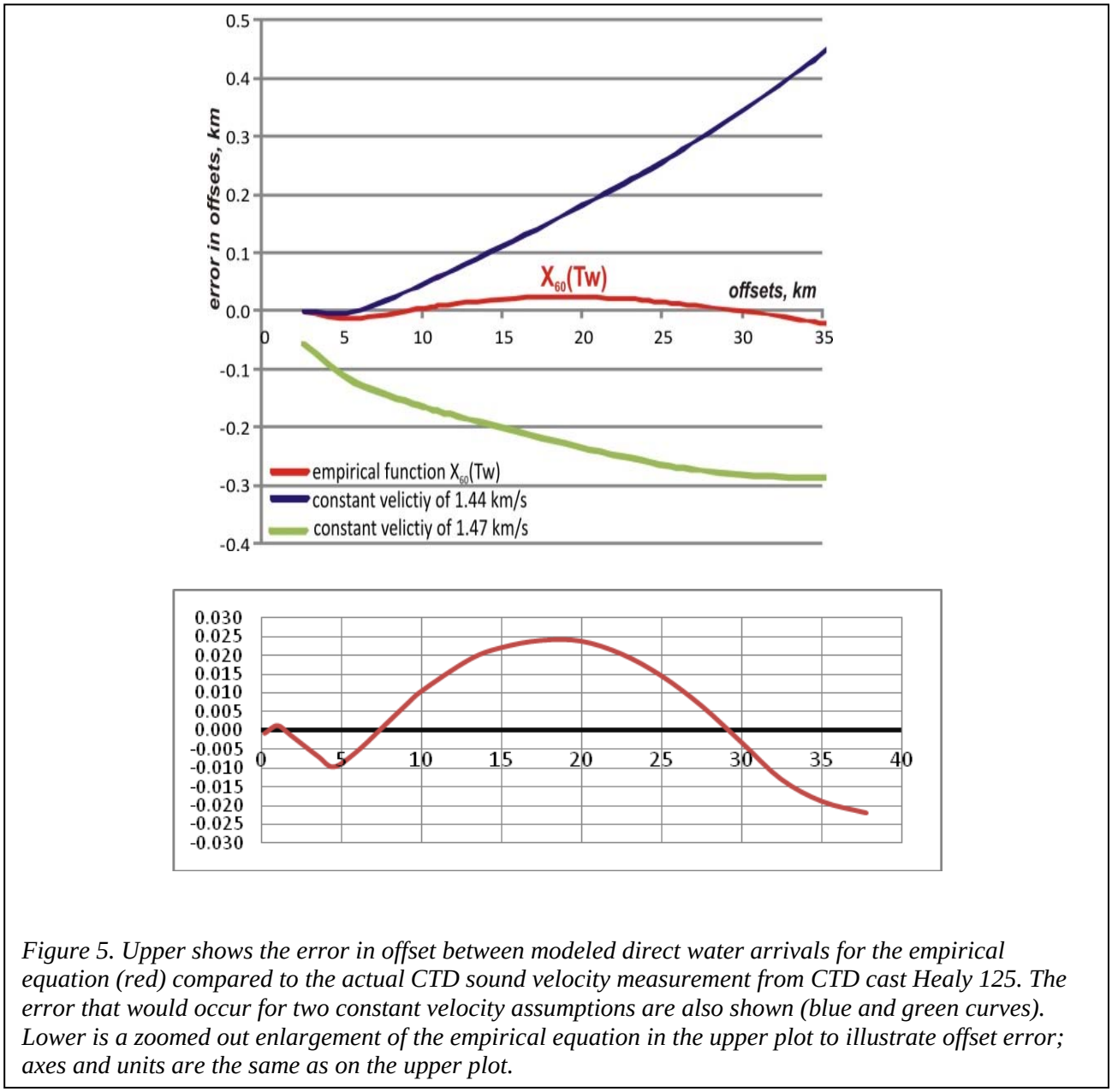

Figure 5. Upper shows the error in offset between modeled direct water arrivals for the empirical equation (red) compared to the actual CTD sound velocity measurement from CTD cast Healy 125. The error that would occur for two constant velocity assumptions are also shown (blue and green curves). Lower is a zoomed out enlargement of the empirical equation in the upper plot to illustrate offset error; axes and units are the same as on the upper plot.

5.2 Direct Water Wave Arrival

Digitizing the travel times of the direct water wave arrivals to provide the input Tw to the empirical equation (see section 4.1) involves several steps. Pre-processing of the sonobuoy data includes correction for the delay between the trigger and airgun firing (either 51 or 57 ms), followed by doubling trace length based on the firing interval (14-20 s). The reason for trace length doubling is because at farther offsets, clear seismic energy, including the direct water wave arrival, continues to arrive after subsequent airgun firings.

The offset assignment process begins by assigning a preliminary offset using the latitude and longitude of the sonobuoy drop location and airgun firing location. In case geographical coordinates are not available in the SEG-Y data, the water wave from the entire trace display is picked and assigned a preliminary offset assuming a constant velocity and linear raypath. Subsequently, the data are displayed using a reduction velocity of either 1.441 or 1.45 km/s (Figure 6) which is the average water velocity at the sea level. Picked values are then overlain onto the data within a small time window (100 ms typically), where small misfits are spotted by the jittery pattern of arrivals and fixed by re-picking the water wave and re-assigning the offsets (Figure 6). This process is repeated until a satisfactory fit is achieved.

To get smooth and accurate phases in the sonobuoy data in the offset-time domain, every trace has to be picked separately. With SeisWide, a semi-automatic picking algorithm was developed, which involves the following computing steps:

- The user determines an estimated optimal digitizing line by mouse drag and drop.
- An average trace is produced in a small time window (~100 ms) immediately after and along the optimal line at a sample interval of ~3 ms. All traces in this time window are extracted in memory, oversampled by a factor of 5 to a sample interval of ~0.6 ms, and then an average trace for this window is computed.
- Each trace in the same window is checked for an optimum time delay against the average trace using a semblance criterion. The computed optimum time delay is applied to each trace, and is repeated for all related traces covered by this drag and drop mouse movement.

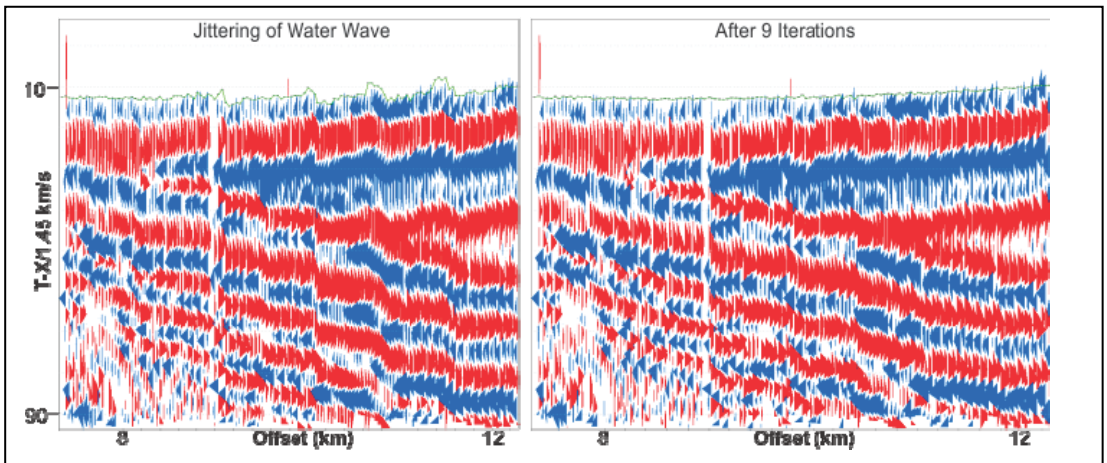

Figure 6. Comparison of initial and final picking of the direct water wave for offsets of 8-12 km for sonobuoy 2007-11. Left shows the alignment of traces for the initial picks using a mouse-assisted automatic picking algorithm. Right shows the same series of traces after nine iterations of picking.

The left panel of Figure 6 shows an example from sonobuoy 2007-11 with an initial pick of the water wave using SeisWide. The right panel shows the result of the automatic picking and assigning offsets. After nine iterations, the overlay of computed travel time shows a nearly perfect match and much of the jittering noise is eliminated. Unfiltered data are found to be most useful for this step. This processing is especially useful in producing a good RMS velocity analysis because it improves the continuity of the wide-angle reflections. The same picking algorithm is also quite useful in picking other phases, such as crustal phases for refraction error analysis.

6 Coincident Multichannel Seismic Reflection Profiles

6.1 Overview

During acquisition of the sonobuoy data, coincident multichannel seismic (MCS) reflection data were also recorded. Details of the acquisition and at-sea processing of these data through preliminary stack and migration have been reported in expedition cruise reports (Jackson and DesRoches, 2010, Mosher et al., 2009, Mosher et al., 2010, Mosher, 2012). The multichannel streamer was a 16 channel, 100-m long solid state system towed from the airgun sled (Mosher et al., 2012). The short streamer length (100 m) and deep-water of the Canada Basin (3.8 km) preclude using these data for velocity analysis. The sonobuoy data, which provide the velocities, utilize the same source as the multichannel data and are therefore directly comparable (see Figure 3). More than 15,000 km of high-resolution profiles were collected between 2007 and 2011 (Figure 7).

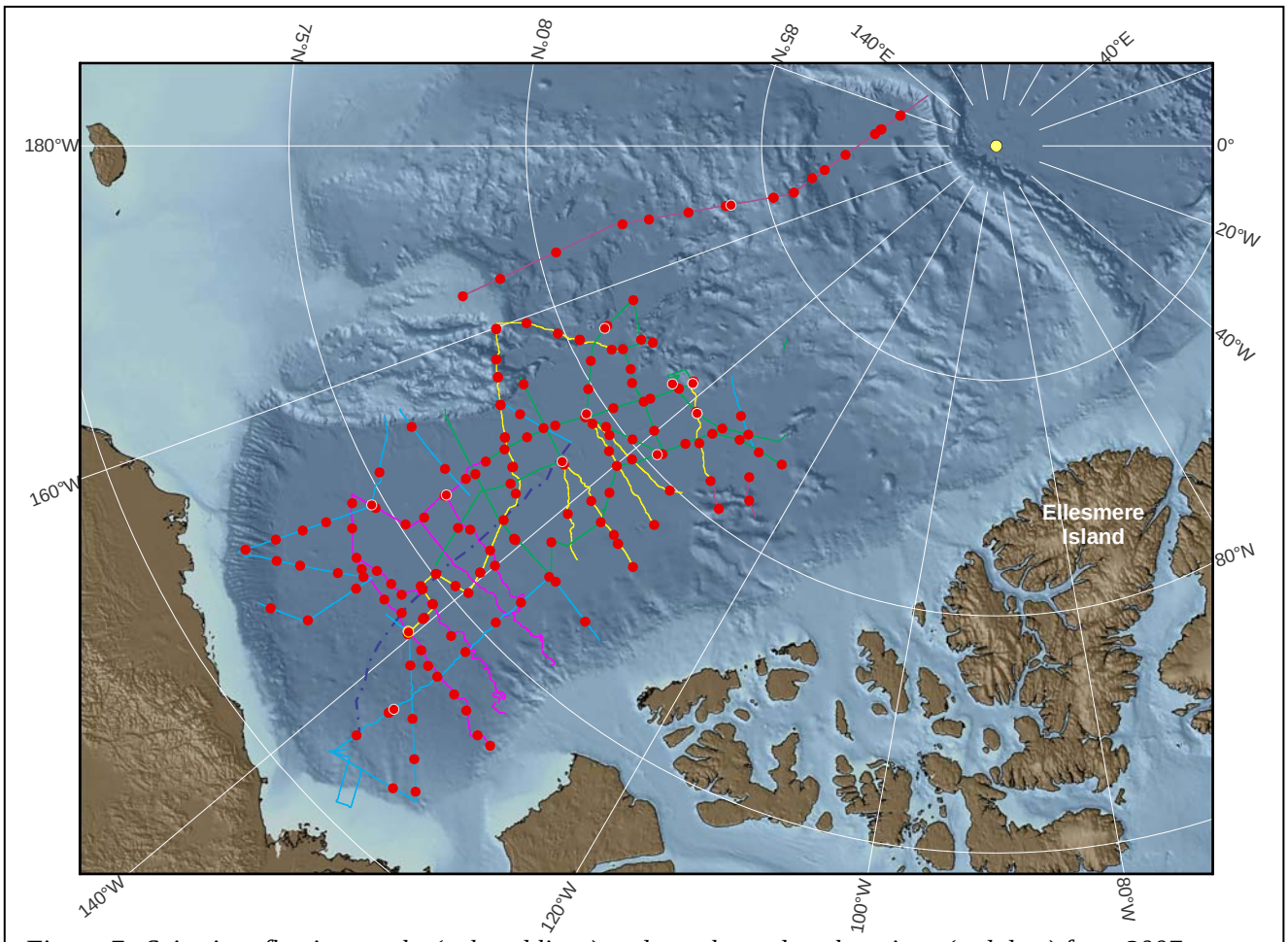

Figure 7. Seismic reflection tracks (colored lines) and sonobuoy drop locations (red dots) from 2007 to 2011 expeditions to Canada Basin.

In general, the at-sea or preliminary processed data were used for the initial constraints in both FM and SA. This atlas only reproduces those sections of the multichannel data that are coincident with the sonobuoy data.

6.2 Data Processing

Seismic reflection data were processed using Claritas seismic processing software. Original SEG-D files were assembled into line segments and converted to SEG-Y format. Shipboard processing was undertaken for quality control purposes and to produce initial datasets for interpretation. Details on the shipboard processing may be found in the relevant cruise reports.

Data quality is generally excellent except where heavy ice conditions required high levels of thrust from the propellers in order to maintain progress through the ice pack. The resulting prop-wash causes high amplitude noise in the 0-25 Hz band that typically contaminates entire shot records, but fortunately only across discrete shotpoint intervals. The noisy shotpoint intervals were most common on records collected during the single-ship operations of 2007, but about 15% of all records from 2007 through 2011 require filtering specifically to attenuate prop-wash noise. Also, on some lines, heavy swell under open ocean conditions introduced significant noise.

Final post-processing sequence of the 2007 through 2011 dataset was as follows:

1. Compile and read SEG-D shot records with trace DC bias removal
2. F-K filter to remove dipping linear noise on shot gathers
3. Apply bandpass filter of 4/7/108/220 Hz
4. Propwash and swell noise attenuation through F-X deconvolution of common receiver gathers
5. Spike and noise-burst editing
6. Minimum phase conversion and bubble pulse elimination
7. Surface related multiple attenuation
8. Geometry assignment including gun and streamer statics
9. Trace equalization
10. CMP sort and stack
11. Final geometry and amplitude recovery
12. Post-stack migration using sedimentary velocity models from sonobuoy analyses
13. Seafloor mute
14. SEG-Y output

7 Forward Modeling (FM) of Refracted Arrivals

7.1 Overview

Refractions are wide-angle seismic phases that travel near-horizontal through layers, with rays originating from the source**,** bending through layers in the Earth according to Snell's Law until they eventually bend upwards back into the water column and are sensed by the sonobuoy recorder. At offsets of 10-40 km in Canada Basin, refractions from various sedimentary layers, the crust, and occasionally from the upper mantle are observed with much stronger amplitudes than reflections. The

exception is when reflections from the mantle occur (PmP arrivals), which are among the strongest amplitude arrivals. Sedimentary refractions are most common in the central and southern Canada Basin, but rarely are observed in the northern Canada Basin near Alpha Ridge, where the sediments are thinnest and high-velocity volcanic rocks associated with the High Arctic Large Igneous Province are inferred to occur (Maher, 2001).

Data from 138 sonobuoys show good signal up to 35-40 km offsets that are appropriate for forward modeling (FM) of refracted arrivals. This section describes the methodology used for the velocity models presented in the page 2 portions of this Atlas for each sonobuoy.

7.2 Traditional Forward Modeling

Forward modeling and ray tracing of the sonobuoy data uses the RAYINVR program of Zelt and Smith (1992) and Zelt and Forsyth (1994) combined with in-house software SeisWide (described below). This method provides a 2-dimensional simulation of Earth structure in distance-depth (or offset-depth, X-Z) domain by specifying up to 30 layers with each layer containing velocity nodes that are bi-linearly interpolated between nodes. The model produces rays that travel through the layers, yielding closely spaced offset-traveltime (T-X) pairs that can be compared with observed arrivals in the sonobuoy data. The model is iteratively revised and raytraced to arrive at the best fit for a final model.

The availability of multichannel seismic reflection profiles along the sonobuoy profile greatly improves the FM technique. Since these data are coincident, the first step in interpreting the offset-corrected data was to geometrically align them with reflection profiles. For simplicity, the sonobuoy is located at 0 km distance on the seismic profile when the ship moves from west to east or north to south directions (i.e., for left to right plotting), or at 35 km distance when ship moves in the opposite direction (i.e. in east-west or south-north directions) for right to left plotting. Major horizons on the reflection profile were digitized to generate a preliminary model in the time domain, with preliminary velocities assigned to each layer.

When a refraction phase is identified for a layer, the phase slope is a direct indicator of interval velocity (V=dX/dT) in the corresponding model layer. However, one of the main intrinsic difficulties in forward modeling is that any updates in velocity will result in depth changes in all underlying layers. This problem can be avoided if the model is updated in the two-way travel time (TWTT) domain, and the model in the depth domain is automatically converted from TWTT domain before ray tracing. In practice, this method enables velocity updates or each layer to be nearly independent from each other during modeling, and the modeling process is greatly simplified and much quicker.

Anisotropy has been tested with some of the sonobuoy data using a revised RAYINVR program, but is ignored in the final modeling because any velocity obtained by refraction (horizontally traveling) phases can be directly used in fitting associated wide angle reflection (near vertically traveling) phases without invoking anisotropy to explain discrepancies.

7.3 Reduced Normal Move-Out Display

For convenience of modeling, we introduce a new transformation (called “Reduced normal move-out or Reduced NMO”) for wide angle data. The main purpose of this transformation is to tie wide-angle events with MCS data at zero offset.

Figure 8 shows the geometry for estimating reduced NMO. The time of each trace in this transformation is reduced by:

$$dT = \frac{\sqrt{X_1^{\,2} + dZ^2} + \sqrt{X_2^{\,2} + dW^2} - 2Z_w + Z_s + Z_g}{V_r} - \frac{Z_s + 2Z_g}{V_w}$$

where X is full offset of each trace from the airgun (Z_g = 0.011 km) to the sonobuoy (Z_s =0.06 km), α= dZ/dW (dimensionless), Z_w is the seafloor depth, V_w is average water velocity above sonobuoy, and V_r is desired reduction velocity. If X = 0, we have $dT = -\frac{Z_s + 2Z_g}{V_w}$, which indicates that in order to align the sonobuoy reflections at zero offset with MCS data, we only need a one-way raypath correction for the sonobuoy depth and a two-way raypath correction for airgun depth below sea surface.

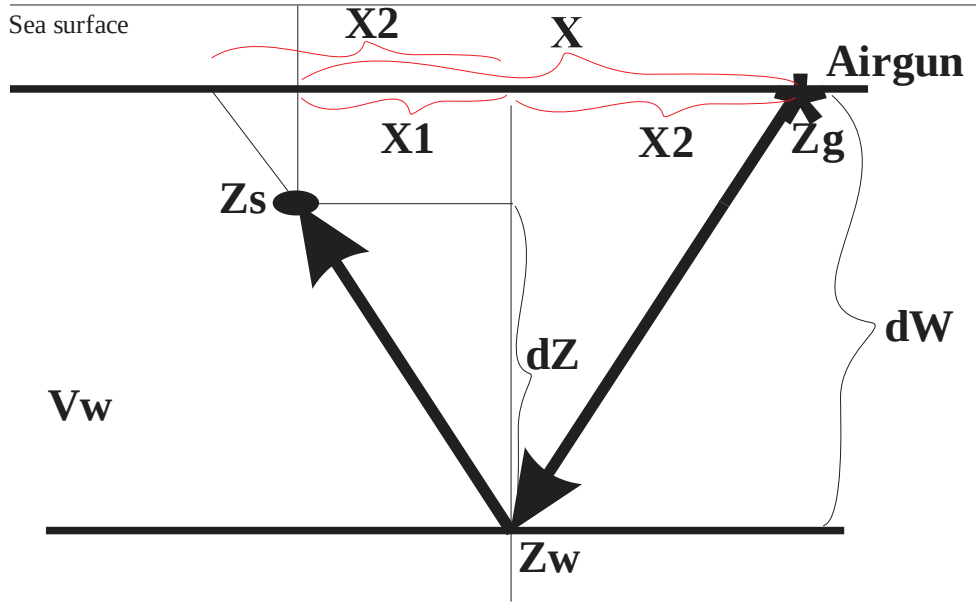

Figure 8. Geometry and variables used in determining reduced NMO. See text for a description of the variables and equations used.

Alternatively, an equally valid approximation to the above formula was used in the work of this Atlas:

$$dT_{avg} = \frac{\sqrt{X_h^{\,2} + dZ^2} + \sqrt{Y^2 + dW^2} - 2Z_w + Z_s + Z_g}{V_r} - \frac{Z_s + 2Z_g}{V_w}$$

where $X_h = X/2$ is half offset, and $Y = X_h / \alpha$. A quick calculation indicates that (dT_{avg} - dT) is always 0 at X = 0, and 0.139 sec at X = 35 km assuming dW = 3.8km, Z_s = 0.06 km. Therefore, the difference is very small in the study area. Both formulae deliver correct results because both the sonobuoy data and computed ray curves were reduced by the same formula. In this Atlas, when Reduced NMO is applicable (to some panels of Page 2) dT_{avg} was used (due to historical reasons).

After this transformation, every reflection event of the sonobuoy data at zero-offset exactly coincides with reflection data in two-way travel time domain. An example of a reduced NMO section with its coincident MCS profile is shown in Figure 9.

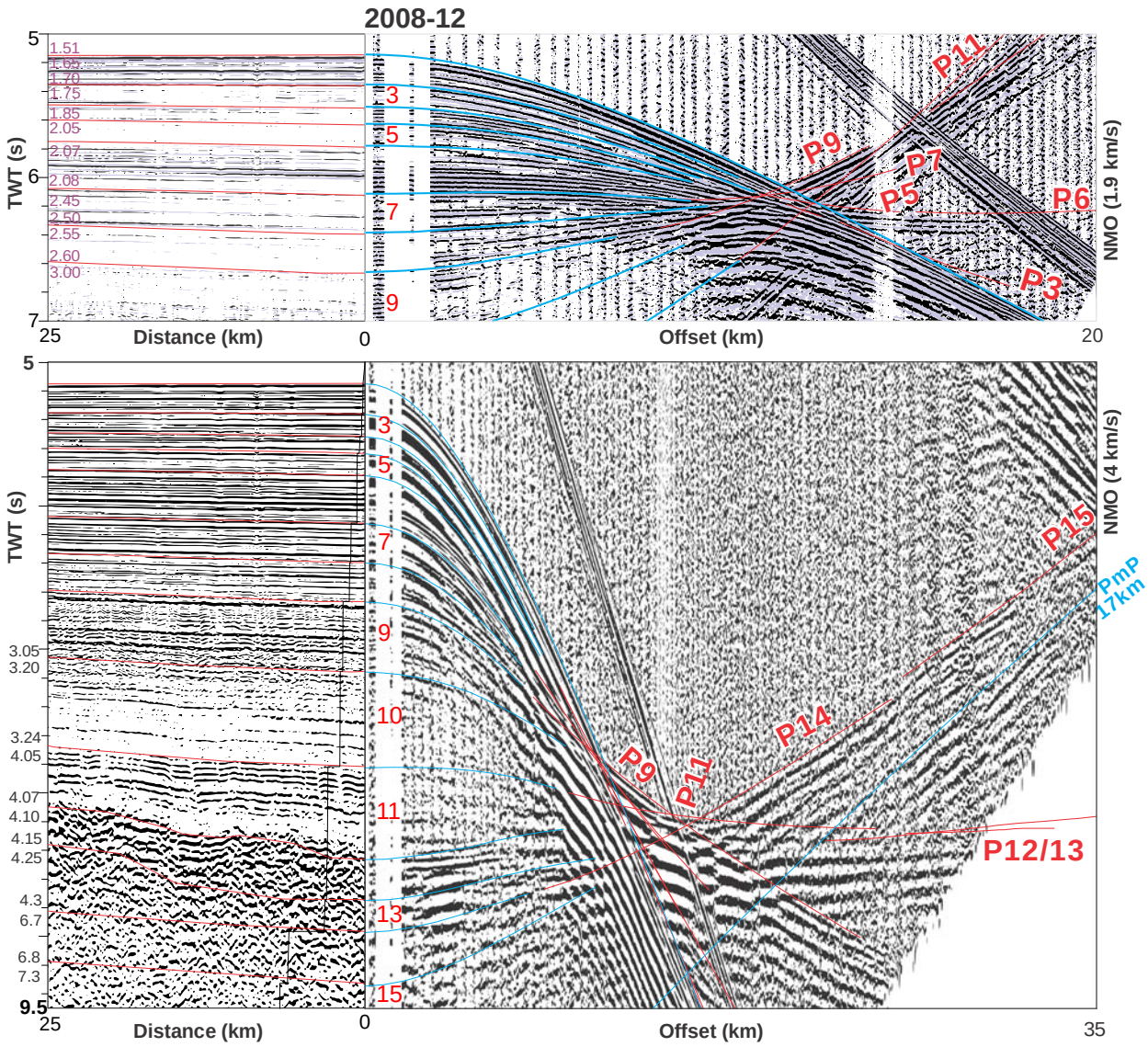

Figure 9. Raytraced sonobuoy 2008-12 (right) with the reduced NMO transformation to coincide with the zero-offset coincident multichannel reflection (MCS) profile (left). Superimposed on the sonobuoy data are computed refractions (red lines) and wide angle reflections (blue lines). Note that every modeled event in the MCS profile is directly connected to wide-angle sonobuoy data at zero offset. Top panels show shallow layers with NMO reduced at smaller velocity than the panels below.

Modeling with reduced NMO has four main advantages:

(a) A direct 1:1 linkage exists for every event of the reflection profile with the corresponding event in the sonobuoy data at zero offset. Thus, every reflection event can be visually traced/linked into the offset domain's wide angle reflection and refraction for the full sonobuoy record.

(b) Details of various phase patterns at wide angles can be revealed by changing the reduction velocity Vr for display (e.g. in Figure 9, Vr = 1.9 km/s for near seafloor events and 4 km/s for deeper sediments).
(c) Small targets (e.g., for oil and gas) can be studied in more detail in the offset domain.
(d) More importantly, many thin sedimentary layers can be revealed this way that are not possible to be seen in conventional refraction modeling methods.

7.4 Model Resolution

7.4.1 Sedimentary Layers

Assuming the two-way travel time (TWTT) of each sedimentary layer boundary is accurate, perturbing the velocity value of each model layer reveals a general velocity resolution of ±1-3 % for a layer in which refractions are observed. For a layer in which no refractions are observed, but for which a layer must exist to explain deeper arrivals, a greater downward velocity gradient usually exists and its bulk velocity resolution, as estimated by fitting the observed wide-angle reflection phase, is in general less than ±7%.

To further quantify the error estimates in sedimentary layers, the velocity values in the time domain can be perturbed, assuming the time of each reflector is accurate in the reflection profile and the modeled water velocity is accurate. The corresponding maximum possible velocity error for each layer is assessed and compiled (Figure 10, top), and the corresponding possible depth error against the layer depth is computed and compiled (Figure 10, bottom). The 14 sonobuoys used in this analysis are distributed throughout the five years of the field programs and are thought to be representative of the geographic distribution of sonobuoys illustrated in Figure 1. Appendix 3 has the table of values used in this resolution analysis.

The resolution associated with the error in velocity is generally less than 4 % but can go up to 7 % (Figure 10, top). The depth resolution is likewise of similar magnitude. If the sonobuoys used in Figure 10 are assumed to be representative for the rest of the sonobuoys in the Canada Basin and its surrounding area, this resolution can be applied to the entire dataset. For example, the basement for sonobuoy 2007-20 is estimated to be at 5.0 km depth below the seafloor. With a 4 % error bound, we get a basement resolution of less than ± 200 m.

In few cases, resolution of velocities and basement depth can be lower than above when data quality is very poor. The readers can refer to individual Page 2 to easily determine this; however, the resolution estimates in this section are believed to be applicable to most of the sonobuoy data in this Atlas.

7.4.2 Crustal Layers

When crustal refractions are observed and modeled, perturbing the crustal velocities suggests an error bound of ± 0.2 km/s for crustal velocities, and ± 1 km for the depth to Moho if it is observed. These values are in general compatible with error estimates for seismic refraction data in other basins of the Arctic (e.g. Lebedeva-Ivanova, 2010; Funck et al., 2011). This similarity is reasonable because, similar to other authors, our sub-crustal structures are deduced only from sonobuoy wide-angle data as the coincident MCS data are not deep enough to be helpful in deciphering deeper structures.

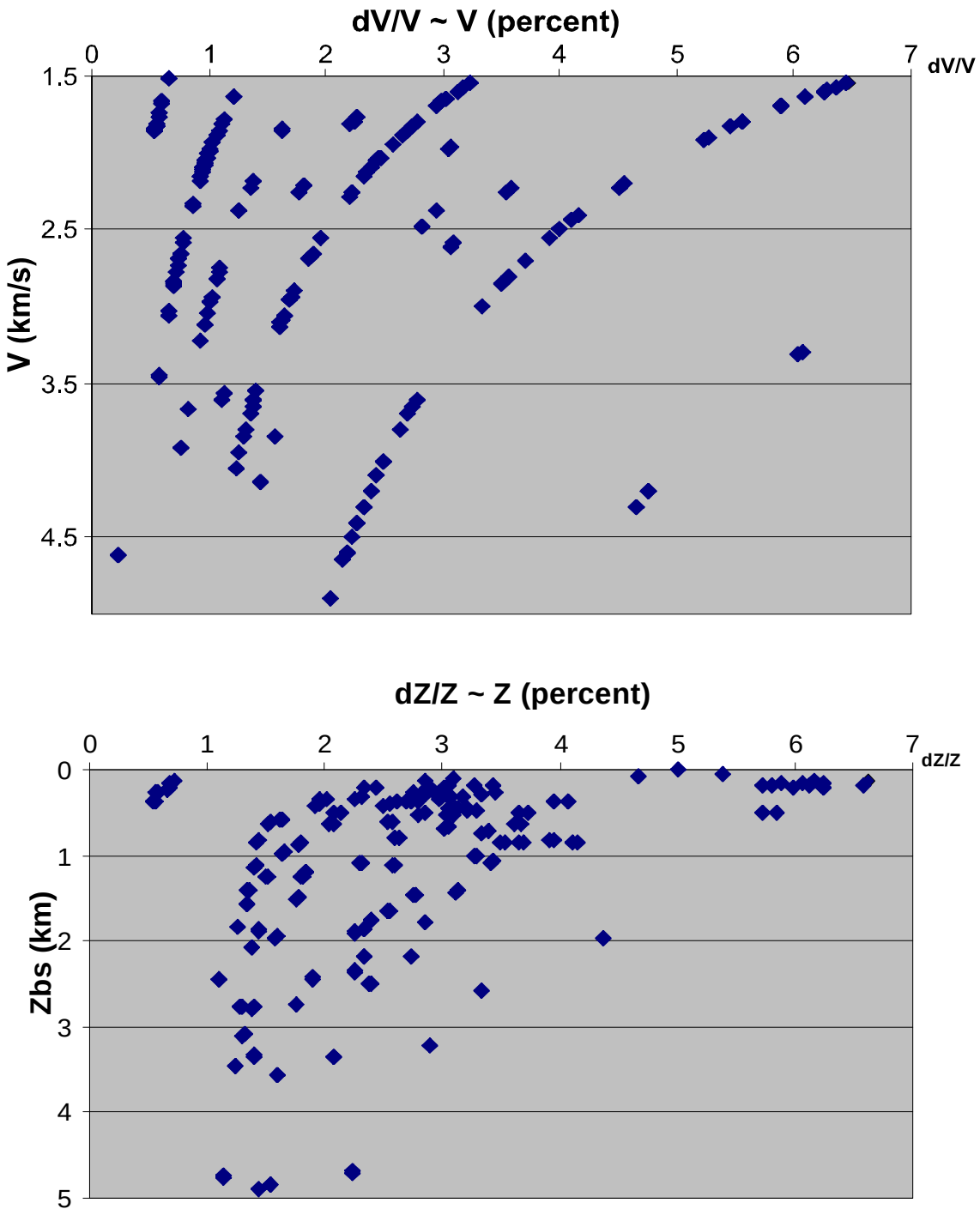

Figure 10. Compilation of velocity (top) and depth (bottom) errors for 14 sonobuoy models, plotted from the spreadsheet data in Appendix 3. For each sonobuoy model, the error analysis is done in the time domain since the time value of each layer is fixed (and accurate) regardless of layer velocities. The steps include: 1) velocity of each layer is perturbed and ray traced until reaching unacceptable misfit with data; 2) complete the list of all velocity error estimates against velocity values (top panel) for all layers; 3) produce two extreme models representing the two error limits based on the list; 4) compute total the depth difference for each layer, against its depth below seafloor (bottom panel). Zbs: depth below seafloor.

7.5 SeisWide Software

The processing methods outlined above are built into our in-house software, SeisWide. SeisWide was created in 1996 using Microsoft Visual C++, and works with a unified graphical manipulation of SEG-Y seismic data (including multichannel seismic reflection data, wide-angle Ocean Bottom Seismometer and sonobuoy profiles) with interactive velocity modeling. The complete software package can be downloaded at http://seiswide.hopto.org/seiswide.zip , with online activation built-in. The open source Fortran raytracing program RAYINVR (Zelt et al., 1992) was revised for proper file inputs and outputs for interfacing with SeisWide. In this combined system, RAYINVR only takes the SeisWide's model, does the raytracing, and output results as disk files, and SeisWide handles all other tasks.

SeisWide handles all the currently needed processing and modeling steps out of field-recorded SEG-Y data. Data processing steps such as automatic water wave picking and offset assigning, distance assignment for multichannel data, filtering (time varying or distance varying), despiking, deconvolution, time-code removal, regular noise reduction, and optimal coherency trace mixing are included in the software. Complete interactive modeling and presentation functions can be done equally well both in time (TWTT) and depth domains. On-screen digitizing is also possible with a versatile and easy-to-use graphical interface. Table 3 gives a list of major relevant functions from the main menu in SeisWide.

Table 3: SeisWide Principal Functions

SeisWide Main Menu	General Menu Items	Important Menu Items
File	Open, Save, Export, Print	▪ **Import Bitmap**: use bitmaps as segy in display and modeling ▪ **Export Bitmap/PDF**: output screen display as bitmap or PDF at user-specified resolution.
Edit	Copy, Label sizes, IBM floating mode, Toggle label …	▪ **Boundary**: editing model boundaries ▪ **Velocity**: editing layer velocities ▪ **Text**: Editing displayed texts
View	Toolbar, Status Bar	▪ **Segy Info**: output detailed segy trace info ▪ **Time Section By Trace**: simple trace display of segy file (wiggle, area fill, color fill et al.) ▪ **Time Section by km**: traditional distance/offset display of segy with given reduction velocity ▪ **Depth Section**: segy display in depth domain, auto converted from time domain ▪ **Velocity Color Map**: colored velocity model display in depth domain ▪ **Both Velocity+Depth Section**: display of segy data on top of color model in depth domain ▪ **Velocity Contours**: contour color display of velocity model ▪ **RMS-Velocity Section**: RMS velocity display from wide-angle data ▪ **Model+Time Section in TWTT**: MCS reflection data overlain by velocity model in time ▪ **NMO-Corrected Section**: Reduced NMO display of wide-angle data ▪ **Sizing of Graph**: change current display size

SeisWide Main Menu	General Menu Items	Important Menu Items
Processing	▪ Trace Re-Order ▪ Chop Data ▪ Split Data ▪ Add Data ▪ Data Resample ▪ Append Segys ▪ Data Debias ▪ Data Normalize ▪ Data Despike ▪ Gain Adjustment ▪ Spherical Correction & Attenuation ▪ Wiener Decon ▪ Trace Balance ▪ Coherency mixing ▪ Some other tools …	▪ **Segy Conversion**: Unix-PC, PC-Unix ▪ **Reverse Signs of Offset**: change offset sign to accommodate ship direction differences ▪ **Shift in Time & Space**: static corrections and horizontal re-positioning of segy data ▪ **Associate km to Trace**: each trace is assigned a distance for modeling, resolution in cm ▪ **Distance Adjustment**: :tune-up for trace distance ▪ **Trace Subtraction**: Noise suppression method ▪ **Coherency Plot**:: mixing of adjacent traces using coherency criteria ▪ **Time-Depth Conversion**: Time-depth conversion using velocity model ▪ **Flatten Segy Along Curve**: for MCS data
Modeling	▪ Load Zelt's Model ▪ Load Reid's Model ▪ Model Tools (add, delete, move, duplicate, anisotropy et al.) ▪ Model Conversions	▪ **Raytrace**: can model S wave, multiple, double refraction. ▪ **Gravity Modeling**: Velocity model converted to density and produce modeled gravity curve ▪ **Subsidence Before Sediment Loading**: strip sediments loading on velocity model ▪ **Flip or Shift Model**: for onscreen model editing ▪ **Produce Synthetic Wide-angle Segy**: Synthetic segy can be used the same way as field records ▪ **Dump V-Z Curves**: Output station meta data, pseudo-well info, converted RMS velocity table, color gridding info. ▪ **Overlay Computed Peglet Linedraw**: for spot multiples on MCS data ▪ **S Wave Labeling**: help model S waves
Digitizing	▪ Start Digitizing ▪ Load Digitizing ▪ New Curve ▪ Shift Digitized Points ▪ Undo point ▪ Save & Show Digitize ▪ Finish Digitizing	▪ **Digitizing Options**: plain text or Zelt's error bar format ▪ **Resize & ivray**: for pick resolution and error analysis
Window	▪ New Window ▪ Cascade ▪ Tile	

SeisWide also utilizes some extensions that differ from standard SEG-Y format:

- Traditional header for trace time delay (short delrt, bytes 108-109, first byte counted as 0) is complemented with another header (int t1, bytes 210-214). A combination both these two headers allows us to describe much greater time delays often required for large offset data while maintaining compatibilities with other industry software.

- A new header (float trcDist, bytes 224-227) stores trace distance and allows model distances to be assigned for as much as thousands of kilometers.

- A new header (float trcOffset, bytes 228-231) stores the decimal part of trace offset and is created to allow for greater resolution than the offset header in standard SEG-Y. Standard SEG-Y specification allows offsets to have a resolution of one meter only.

8 Semblance Velocity Analysis (SA) of Wide Angle Reflections

8.1 General Overview

Semblance velocity analysis has been traditionally applied to multi-channel seismic reflection surveys. This method commonly assumes a one dimensional (1D) structure, scans all the possible root-mean-square (RMS) velocity spectrum at a given common mid point (CMP) trace gather, and pick the strongest point that correlates with the maximum semblance on the velocity spectrum plot (Yilmaz, 1987). Here, we try to apply this procedure to the sonobuoy wide angle data. The standard seismic processing tools in the commercial package ProMAX® were used for processing the data and conducting semblance velocity analysis.

There are a number of motivations for implementing SA of the sedimentary section independently of refraction modeling. These are:

- SA is a quick way to implement production-mode analysis for sedimentary velocities in sub-horizontal strata.
- The multichannel data are available to be used as a guide for identifying the main reflections and picking velocities.
- Short offset records of sonobuoys (i.e., less than ~12km, but longer than ~6 km) are generally unsuitable for forward refraction modeling (FM) but can still be used for SA.
- Estimated velocities and depths from SA can be merged with FM for a more comprehensive interpretation of the sedimentary cover.

The SA technique can also be applied to wide-angle reflection records such as recorded by sonobuoys. NMO velocity is equal to the RMS velocity for flat-lying horizontal units, which can be easily transformed into interval velocity (Dix, 1955). For regions such as the central and southern Canada Basin, with sub-horizontal sediments and little tectonic disturbance (e.g., Mosher et al., 2012), SA is appropriate to apply to the large offset sonobuoy data that satisfy the assumptions of horizontality. Velocities were not picked on dipping reflection surfaces nor were semblance analyses done along the margins where the seafloor was dipping and horizons are characterized by rough morphology due to mass transport deposits (Mosher et al., 2012).

Data from 104 sonobuoys from 2007-2010 field programs were used for semblance analysis of the wide angle reflected arrivals. This section describes the methodology used for the velocity models presented in the upper panel of page 3 of the Atlas for each sonobuoy.

8.2 Pre-processing Synthetic tests

A series of tests on synthetic data were developed to determine the optimal offsets for using semblance analysis prior to applying it to real data sets (Figure 11). A preliminary velocity-depth model of sedimentary cover in the Canada Basin was constrained by modeling refracted waves and from previous research (e.g. Grantz et al., 2011 and references therein). Synthetic sonobuoy data were generated using the Zelt and Smith (1992) algorithm based on this model. The synthetic data were created using acquisition parameters of the sonobuoy data in 2007-2010. Synthetic data were attributed as a common mid-point gather, and then SA was performed with the ProMAX® semblance velocity analysis tool using different offsets until the analysis most accurately reproduced the velocity-depth model. The test results of these tests showed that offsets from 0 to 7 km are optimal for the SA technique (Figure 11). Traces of the real sonobuoy records at offsets of less than 700 m were generally not useable due to oversaturation of the signal. No attempt was made to correct the oversaturation

because relative offset error on the shorter offsets are greatest, partly caused by excessive noise from the airgun activity and ship movements. Therefore, only offsets of ~0.7-7 km were used in the final SA. This lack of near offsets only slightly affects the quality of the semblance image, since the semblance analysis tool automatically extrapolates results for zero offsets.

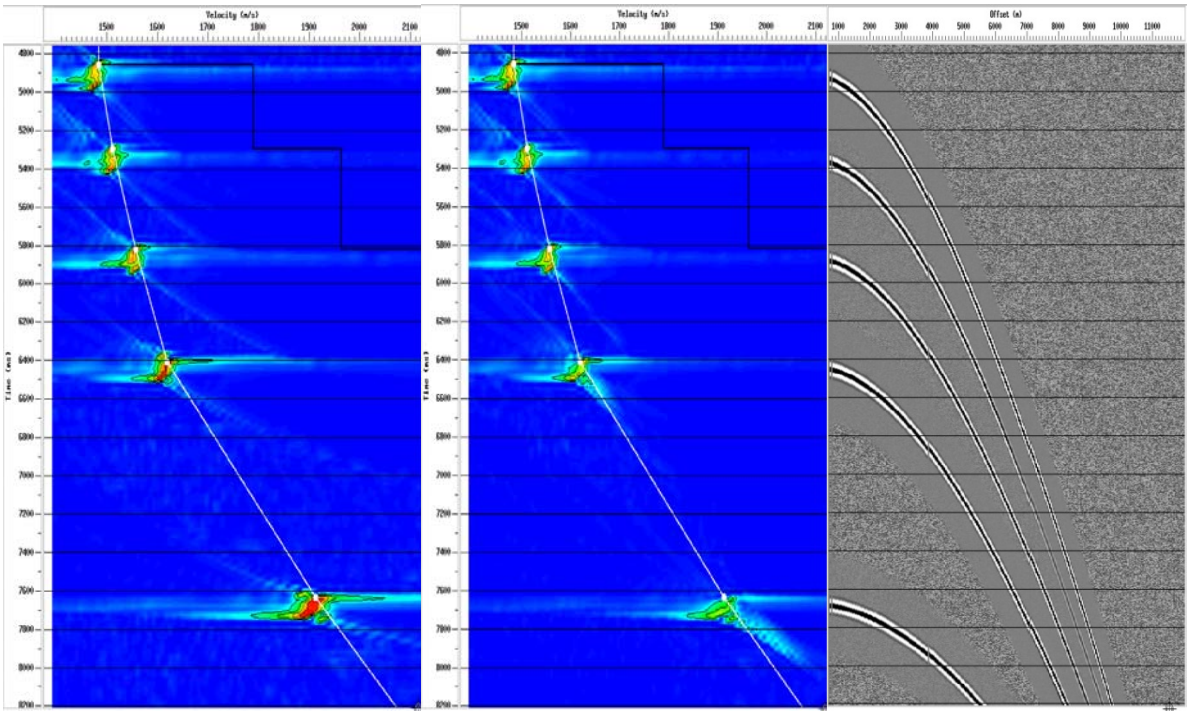

Figure 11. Semblance velocity analysis for offsets of 7km (left panel) and of 12km (central panel) for synthetic seismic data for (right panel). White points show the actual RMS and time of model for synthetic data.

8.3 Processing flow of the sonobuoy data

Processing of the sonobuoy records for semblance velocity analysis is divided into two sequences: (i) steps applied to edit, assign offsets, and generally improve the signal-to-noise ratios of the sonobuoy record for all offsets, and (ii) steps that are specific to the velocity analysis at the 0.7-7 km gathers with subsequent SA to determine interval velocities and depth conversions. This flow primarily focused to improve the wide-angle reflections of the sonobuoy data. The flow was designed with similar parameters as the MCS data processing (Jackson and DeRoches, 2010; Mosher et al. 2009) for easy comparison of both data sets. All parameters of the data processing flow are given in detail in Table 4.

After noise spike removal algorithm was applied to the raw sonobuoy data, the direct water wave arrival times were interactively picked and source-receiver offsets estimated using the $X(T_w)$ function described under the section “Shot-Sonobuoy Offset Determination”. This part of the data processing was done using SeisWide software (see above).

Subsequent data processing steps (Table 4, steps 1.6-1.13) were designed to be stable, simple and applicable for the bulk of the sonobuoy records where offsets, distance between traces, geological structures at the sonobuoy location and other parameters could be quite variable. These processing

steps included a broad minimum phase bandpass filter, predictive deconvolution for the entire length of the trace, and time and spatially variant minimum phase bandpass filter with minor parameter adjustments in accordance for each sonobuoy record.

Table 4. Steps of sonobuoy data processing for SA

Step No.	Processing step	Parameters	Software Used
1.	***For the whole sonobuoy data set***		
1.1.	Static corrections	-51 ms for gun firing delay	SeisWide
1.2.	Assigning offsets	Empirical function (*see text above*)	SeisWide
1.3.	Assigning sonobuoy geometry as CDP gather		ProMAX®
1.4.	Static corrections	+34 ms adjusts the sonobuoy record to account for the difference in the source depth (11 m) and the receiver hydrophone depth (60 m).	ProMAX®
1.5.	Kill bad traces		ProMAX®
1.6.	Trace Equalization	mean scaling for the entire length of the trace	ProMAX®
1.7.	True Amplitude Recovery	constant db/sec correction - 0.5 for the entire length of the trace	ProMAX®
1.8.	Ensemble Balance	mean scaling for the entire length of the trace	ProMAX®
1.9.	F-K filter	reject fun filters velocity m/s -100/1000 frequency 2-90 Hz	ProMAX®
1.10.	Minimum phase bandpass filter	2/3-80/120 Hz	ProMAX®
1.11.	Minimum predictive deconvolution for the entire length of the trace	operator length: 220 ms prediction distance: 38 ms	ProMAX®
1.12.	Time and spatially variant minimum phase bandpass filter	~0-2 s bsf: 7/10-40/50 Hz ~3 s bsf and deeper: 3/5.5-20/35 Hz	ProMAX®
1.13.	Phase correction for the entire length of the trace	decon operator length: 60 ms	ProMAX®
2.	***For sonobuoy data at 0-7 km offsets***		
2.1	Top trace muting	for sea floor reflection	ProMAX®
2.2	AGC	mean, 1000s window	ProMAX®
2.3	Semblance velocity analysis for main reflective horizons with time step >200ms, avoiding low velocity interpretation	sample rate 20 ms calculation window 40	ProMAX®
2.4	Conversion of TWTT and RMS-velocity into TWTT bsl, interval velocity, depth and depth bsl.	Dix equation	ProMAX®

The second sequence of steps of the sonobuoy data processing was applied to offsets up to 7 km. The multichannel reflection data at sonobuoy locations were used as a guideline for this process (Figure 12a). Arrivals before the first reflections were muted, and an automatic gain control was applied for improving the semblance image (Table 4, steps 2.1-2.3 and Figure 12c). Semblance velocities (i.e.,

RMS) were consistently picked at clear high–coherency events on the semblance plots for layers not thinner then ~200 ms TWTT (Figure 12b). The RMS velocities were picked to yield only increasing interval velocities and picking stopped at or above basement on the multichannel record or at dipping interfaces. Velocities were not picked on dipping reflection surfaces that violated our assumptions of horizontality. NMO corrections were applied to the sonobuoy data for quality control (Figure 12d).

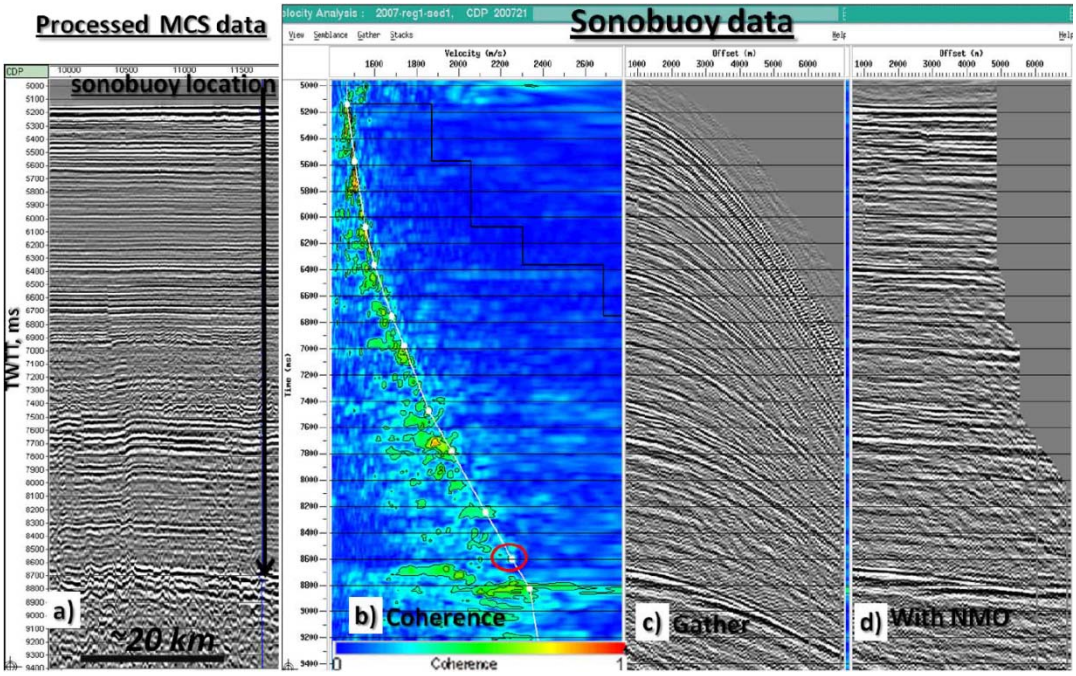

Figure 12. Example of semblance velocity analysis for Sonobuoy 2007-21. a) part of the multichannel line at the sonobuoy location. b) semblance panel showing picked RMS velocities in m/s (white dots and white line), the last reliable pick is marked by red oval; black isolines marks semblance with step of 0.1 in between from 0.5 or 0.6 and higher; color bar showing coherence is located below the panel. c) processed sonobuoy record used for semblance analysis. d) the same sonobuoy record with NMO correction applied.

Unfortunately, deconvolution (step 1.11 in Table 4) did not entirely recover the signal due to variability in the seismic wavelet with the offset caused by source and receiver ghosts and source signature variations. After processing, each reflection was still composed of more than one phase up to about the first second of travel time beneath the seafloor. Therefore, the top of the maximum of the semblance coherence was picked for velocity estimates rather than the center of the maximum.

TWTT and RMS velocity picks were converted to interval velocities and depths using the Dix equation (Dix, 1955); then depths and TWTT were leveled to the sea floor giving depth below sea floor (bsf) and TWTT bsf. The depths below seafloor are equivalent to sediment thickness for the sedimentary section.

8.4 Error analysis

Error in interval velocities estimated by semblance velocity analysis is dependent on data quality. Error also increases with decreasing thickness of the layer in TWTT, therefore only layers thicker than

~200 ms TWTT were picked. Analysis shows that the error in interval velocity calculations may have a magnitude up to 10-15%; however, those errors do not propagate through the entire section since the error in interval velocity within one layer is compensated by error in the next layer of similar magnitude but with opposite signature. Therefore, errors in depth estimates have been analyzed to be less than ~7%.

9 Comparison of Velocity Results

9.1 Individual Sonobuoys

Velocity results from forward modeling (FM) and semblance analysis (SA) were compared in the lower panel of page 3 for each sonobuoy of this Atlas. A sample comparison is shown in Figure 13 using FA results in blu and SA results in red. Interval and RMS velocities are directly comparable in one plot (Figure 13, left) and associated time-depth functions are compared in another (Figure 13, right). The points of the time-depth function are connected to yield time-depth curves in these plots, so these lines do not represent mathematically derived curves. The semblance analysis ends just above basement in this example, and the deeper refractions with velocities up to >6 km/s are also shown.

Figure 13 shows the excellent agreement between the RMS and time-depth curves for sonobuoy 2007-12. The interval velocity curves show discrepancies that are the result of differences in model picks (particularly the existence of gradients that can be used in the forward modeling) and in different depths at which picks are made, which is often a function of individual picking technique.

9.2 Entire Sonobuoy Data Set

The entire sonobuoy data set provides sufficient statistics to be able to compare results from the common sonobuoys. There are 99 sonobuoys that have velocity estimates from both forward modeling and semblance analysis. In order to remove the step-function shape of the interval velocity data, a new interval velocity value is calculated from each adjacent interval velocity pair by mathematically taking the mid-point velocity and the mid-point in time or depth between the two pairs. This is equivalent to assigning the average interval velocity to the middle of the layer. Within this subset of values from common sonobuoys, the deepest semblance pick comes from ~3.7 s TWTT below the seafloor, and the maximum velocity is ~4.5 km/s. Using this travel time as the cutoff for including the interval velocity pairs from forward modeling yields datasets for which there are 656 and 742 velocity-time pairs for semblance and forward modeling respectively.

This subset of velocity-time pairs can be compared in a quantile plot. A distribution of the interval velocities is defined for each technique yielding a representative interval velocity for each quantile of the distribution. A plot of respective interval velocities for the same quantile units can then be plotted to compare the distributions. Identical distributions of data in quantile plots should lie along the 45^{o} line x = y.

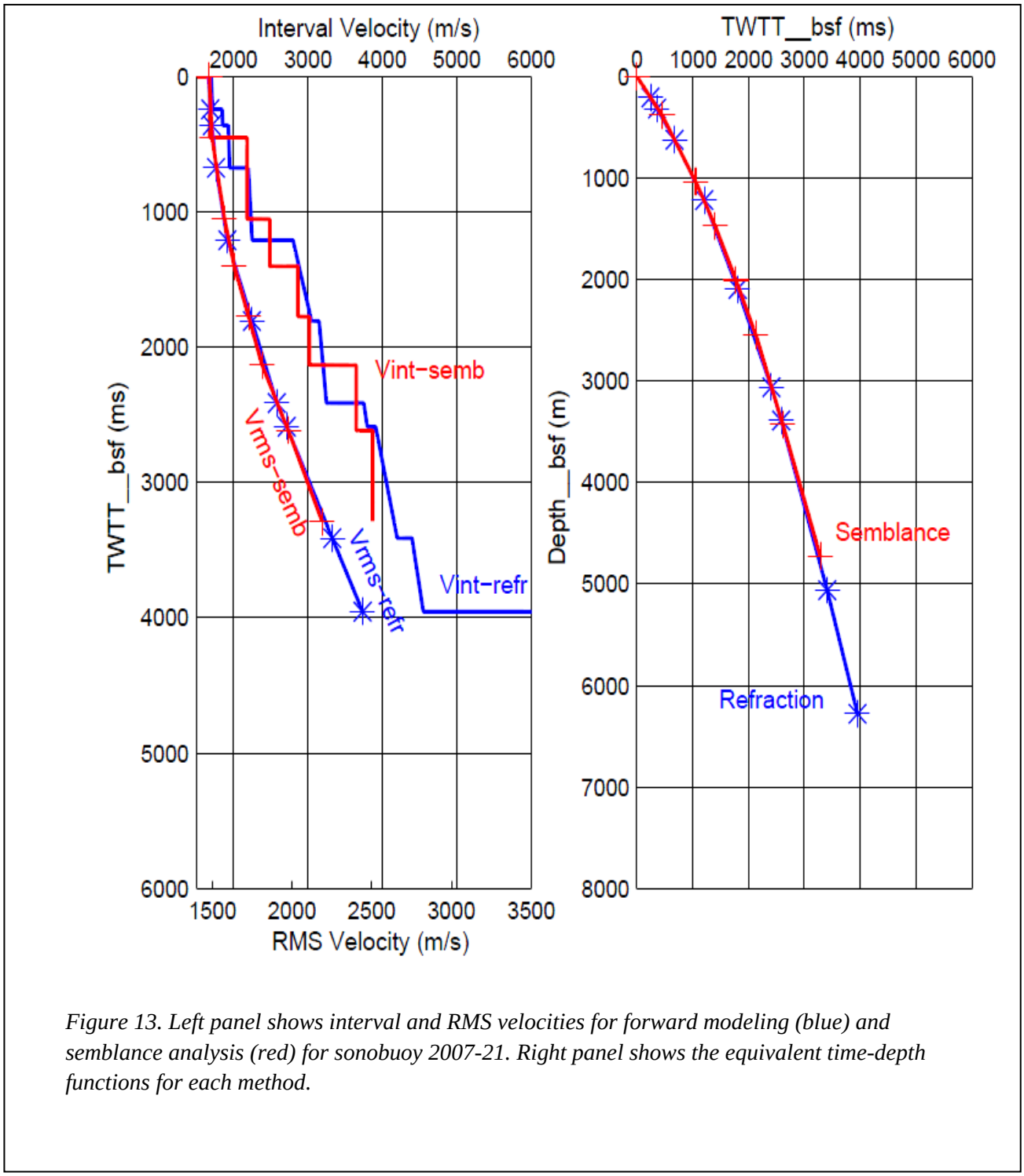

Figure 13. Left panel shows interval and RMS velocities for forward modeling (blue) and semblance analysis (red) for sonobuoy 2007-21. Right panel shows the equivalent time-depth functions for each method.

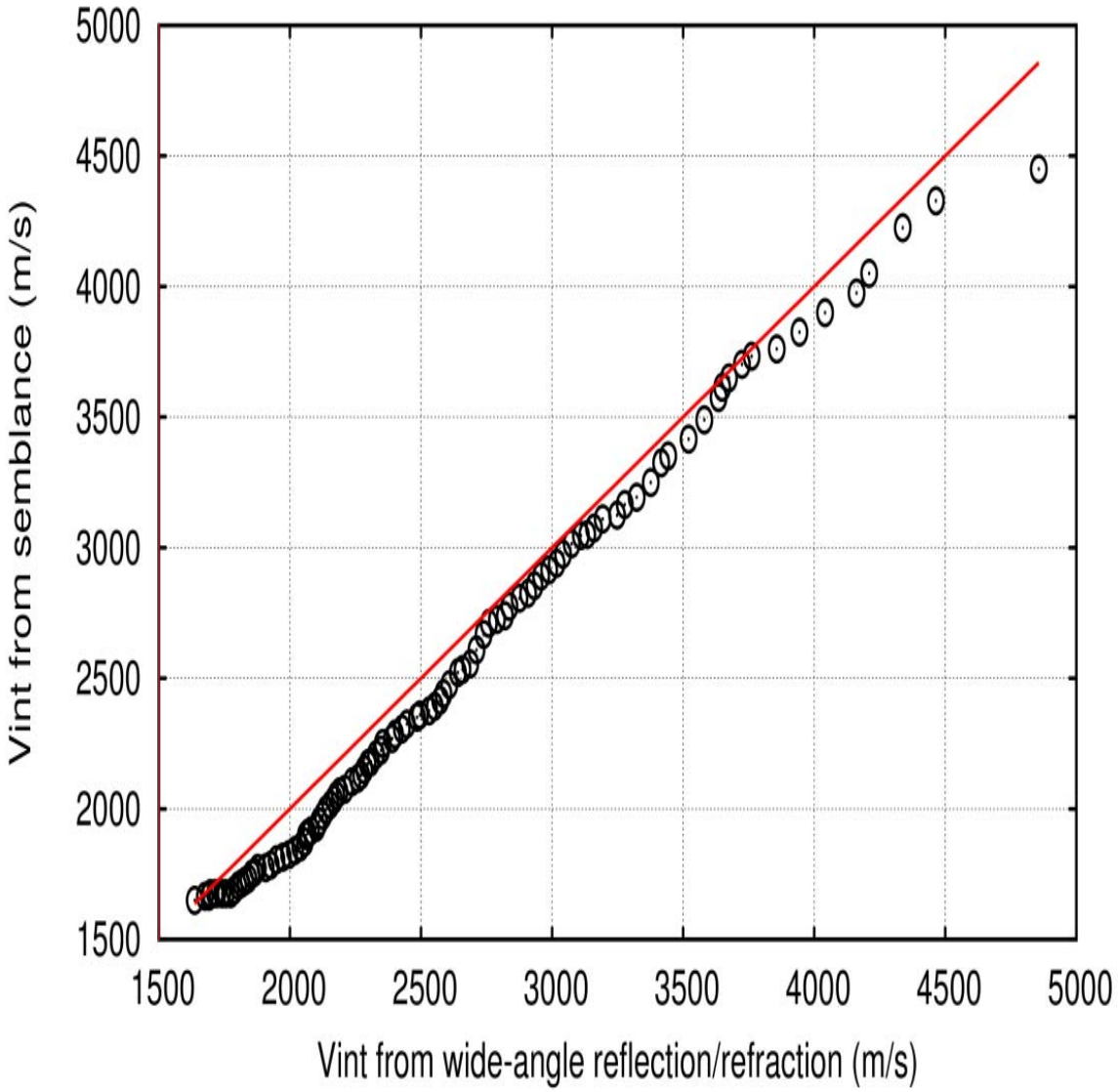

Figure 14: Q-Q plot comparing interval velocities from FM and SA. In this plot, the SA velocities consistently plot slightly lower than the equivalent FM velocities. The red line represents a perfect match (i.e. x-y) between the two techniques.

A quantile plot of comparing the common Canada Basin interval velocities from forward modeling and semblance analysis shows close agreement, but not identical agreement (Figure 14). The Q-Q comparison demonstrates that the interval velocities consistently plot slightly below the x=y line, indicating that the SA values are consistently slightly higher velocity than the FM refraction velocities. Another way to view the comparison is to look at the ratio of equivalent interval velocities (Figure 15). This ratio plot indicates the largest difference between interval velocities is about 10 % (ratio of 1.1) and more than half of the velocities are within 5 % of each other. A possible existence of anisotropy cannot explain this since it would imply $V_{semb}/V_{wide} < 1$ instead of >1 as observed, and neither any static shifts can compensate for the difference. We suggest that such small difference of results may be intrinsic to the FM and SA methodologies, and further studies are needed to verify or correct for the observed differences.

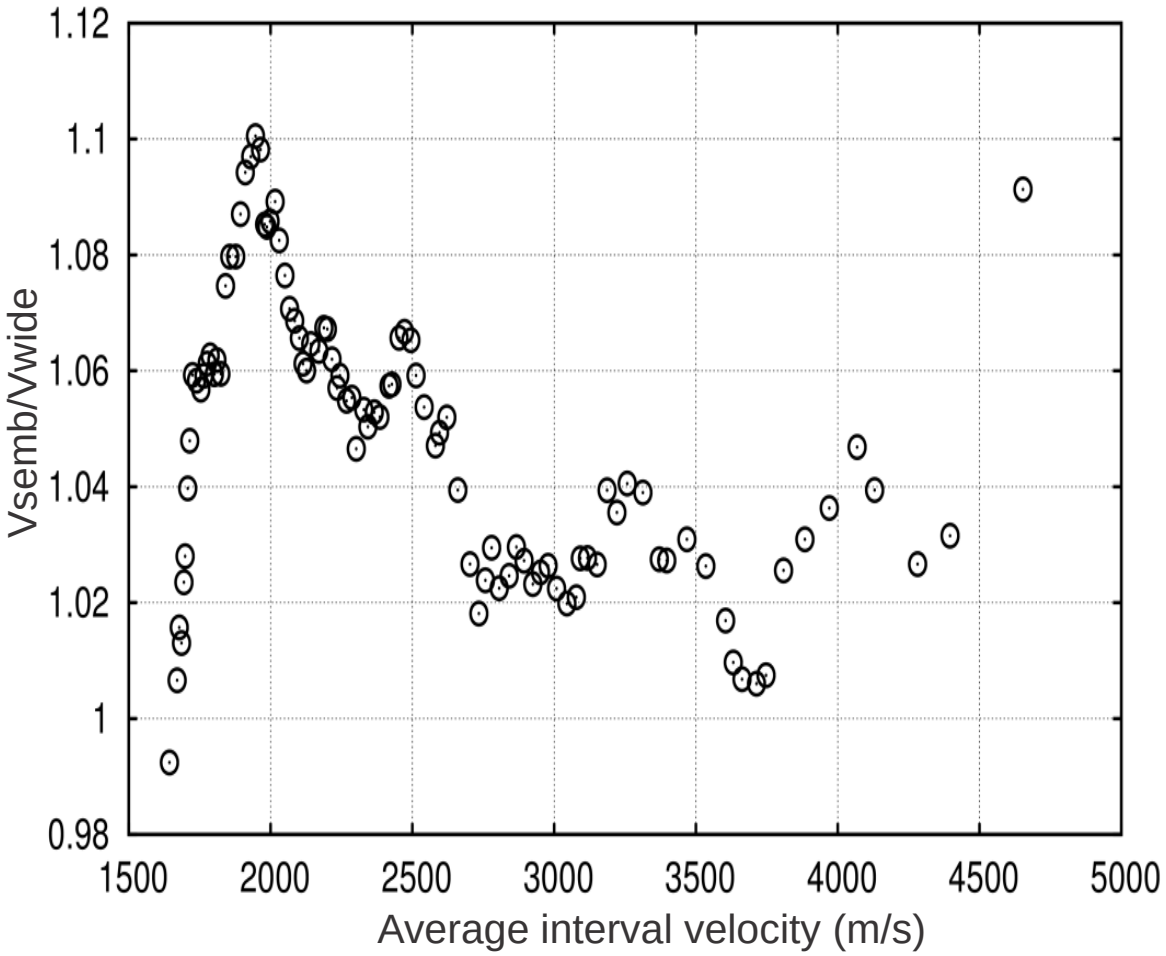

Figure 15. Ratio of FM interval velocities to SA interval velocities using the quantile values from Figure 14. Values of >1 indicate that the SA velocities are higher than the FM velocities.

10 Summary

This Atlas presents the data and velocity models for 144 out of 174 sonobuoys deployed in the Canada Basin during field programs between 2007 and 2011. Two independent methods were used to derive velocities, forward modeling (FM) of refracted arrivals (utilizing offsets up to 35-40 km) and semblance analysis (SA) of wide angle reflected arrivals (utilizing offsets up to 7 km). Forward modeling was done on 138 sonobuoys from all five years of field programs (i.e., 2007-2011); semblance analysis was done on 104 sonobuoys for the first four of the five field programs (i.e., 2007-2010). A total of 99 sonobuoy records were analyzed for both FM and SA. Figure 16 shows a map with all these sonobuoy locations hyperlinked to their respective Pages 1-3.

The two data sets have overlapping velocity solutions primarily for the sedimentary successions. Agreement between the two data sets is excellent. A plot comparing interval velocities from the travel times in which the measurements overlap indicates the maximum difference between the methods is about 10 % and more than half of the measurements agree to within 5 %.

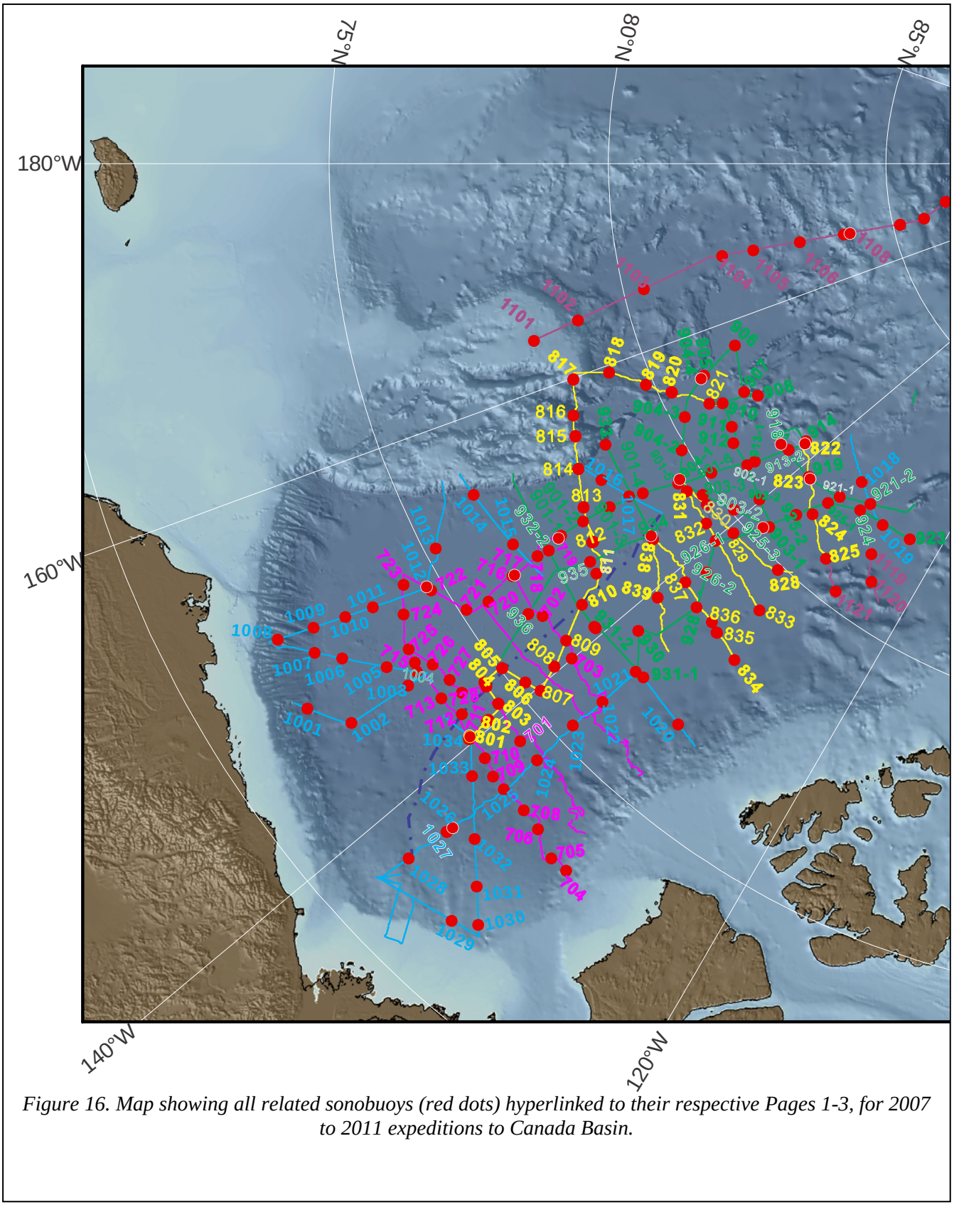

Figure 16. Map showing all related sonobuoys (red dots) hyperlinked to their respective Pages 1-3, for 2007 to 2011 expeditions to Canada Basin.

11 References

Dix, C.H., 1955. Seismic velocities from surface measurements, Geophysics, 20, 68-86.

Funck, T., Jackson, H.R., and Shimeld, J., 2011, The crustal structure of the Alpha Ridge at the transition to the Canadian Polar Margin: Results from a seismic refraction experiment: Journal of Geophysical Research, 116, 26 pp., doi:10.1029/2011JB008411.

Gavrilov A.N. and Mikhalevsky P.N., 2002. " Recent results of the ACOUS (Arctic Climate Observations using Underwater Sound) Program", Acta Acustica united with Acustica, v.88, No.5, pp.783-791

Grantz A., Hart P., Childers V., 2011, Geology and tectonic development of the Amerasia and Canada Basins, Arctic Ocean, in A.M. Spencer, D. Gautier, A. Stoupakova, A. Embry, K. Sorensen eds., Arctic Petroleum Geology, vol. 35 Geological Society, London Memoirs, 771–799.

Johnston, R.C., Reed, D.H. and Desler, J.F., 1988. Special report on marine seismic energy source standards. Geophysics, 53:566-575.

Jackson, H.R. and DesRoches, K.J., 2010, 2008 Louis S. St-Laurent Field Report, August 22 - October 3, 2008, Geological Survey of Canada, Open File 6275, 184 p.

Kutschale, H., 1969. Arctic hydroacoustics. In Monson, A. and Sater, J., editors, Proceedings of the U.S. Naval Arctic Research Laboratory Dedication Symposium, volume 2, pages 246–264.

Lebedeva-Ivanova, 2010, Geophysical studies bearing on the origin of the Arctic Basin, Acta Universitatis Upsaliensis, Digital Comprehensive Summaries of Uppsala Dissertations from the faculty of Science and Technology 729, 79pp. Uppsala, ISBN 978-91-554-7771-4.

Lebedeva-Ivanova N. and Lizarralde D., 2011. An empirical direct-wave travel time equation for Arctic sonobuoy data, The Sixth International Conference on Arctic Margins, abstract.

Maher, H.D., 2001, Manifestations of the Cretaceous High Arctic Large Igneous Province in Svalbard, The Journal of Geology, v. 109, p. 91–104.

Mosher, D.C., Shimeld, J.W., Hutchinson, D.R., 2009. 2009 Canada Basin seismic reflection and refraction survey, western Arctic Ocean: CCGS Louis S. St-Laurent expedition report, Geological Survey of Canada Open File 6343, 266 pp.

Mosher, D.C., Shimeld, J., and Chapman, B.C., 2010, 2010 Canada Basin seismic reflection and refraction survey, western Canada Basin Seismic Reflection and Refraction Survey, western Arctic Ocean: CCGS Louis S. St-Laurent expedition report: Geological Survey of Canada Open File Report 6720, 240 pp.

Mosher, D.C., Shimeld, J., Hutchinson, D., Lebedeva-Ivanova, N. and Chapman, C.B., 2012. Submarine Landslides in Arctic Sedimentation: Canada Basin. In: Yamada, Y., Kawamura, K., Ikehara, K., Ogawa, Y., Urgeles, R., Mosher, D., Chaytor, J. and Strasser M. (ed.) Advances in Natural and Technological Hazards Research, Springer, V 31, pp 147-157.

Yilmaz, O., 1987, Seismic Data Processing, Investigations in Geophysics Series, Volume 2, S.M. Doherty (Editor), Society of Exploration Geophysicists, 526 p.

Zelt, C. A. and Forsyth, D. A., 1994, Modeling wide-angle seismic data for crustal structure: southeastern Grenville province, J. Geophys. Res., 99, 11687-11704.

Zelt, C.A. and Smith, R.B. 1992, Seismic traveltime inversion for 2-D crustal structure. Geophysical Journal International, 108, 16–34.

12 Acknowledgments

This work would not have been possible without the work and dedication of many individuals and organizations. First and foremost, we thank Dr. Jacob Verhoef for spearheading the Canadian Extended Continental Shelf Mapping program from its beginning. He strongly supported acquisition of data throughout the Arctic and recognized the broader value of these data than its primary purpose. The shipboard technicians kept equipment running in some of the most difficult conditions in the world – to them we owe a huge debt of gratitude. We thank the officers and crews of the CCGS *Louis S. St-Laurent* and the USCGC *Healy*. Their collaborative spirit and dedication to service allowed acquisition of these data. Special acknowledgements to Deborah Hutchinson[1], David Mosher[2], John Shimeld[2], Ruth Jackson[2], Matthew Arsenault[1], John Evangelatos[2], Sara Greenberg[1], Kai Boggild[2], Gordon Oakey[2], and Kevin DesRoches[2] for their help in acquisition and analysis of the data that went into this Atlas, and for their scientific and technical reviews. Funding for this work was provided in part by the U.S. Geological Survey as part of the U.S. Extended Continental Shelf Program. Any use of trade names is for descriptive purposes only and does not constitute endorsement by either the Canadian or U.S government agencies.

[1] U.S. Geological Survey, Woods Hole, MA

[2] Geological Survey of Canada, Dartmouth, Nova Scotia

Appendix 1: Table of Forward Modeling (FM) Results

Table of forward modeling results. See Excel file GSCOF7661_Appendix1_ForwardModelingTable.xls

Appendix 2: Table of Semblance Analysis (SA) Results

Table of semblance analysis results. See Excel file GSCOF7661_Appendix2_SemblanceTable.xls

Appendix 3: Sensitivity analysis of selected sonobuoys

The table 3-1 in this appendix gives the velocity and depth values used in estimating the respective errors/resolution of the sonobuoy data set that is plotted in Figure 10 in the main body of the text.

Table 3-1: Sensitivity analysis of selected sonobuoys. VEL and VEL2 are lower and upper bounds of velocities in each layer. DV/V is the percentage of maximum possible error (±dV) of velocity estimate. Similarly, DEPTH, DEPTH2 and DZ/Z are lower, upper and percentage depth error of top and lower boundary estimates of each layer. Zbs: depth below seafloor. See text in section 7.4 for more details.

Sonobuoy	VEL km/s	VEL2 km/s	DV/V	DEPTH km	DEPTH2 km	DZ/Z	Zbs km	±dV km/s	Layer No.
2007-11	1.44	1.44		0	0				
2007-11	1.513	1.513		3.553	3.553				
2007-11	1.57	1.77	6.369427	3.563	3.563		0.01	0.1	2
2007-11	1.59	1.79	6.289308	3.718	3.738	6.060606	0.165	0.1	2
2007-11	1.78	1.82	1.123596	3.728	3.748	5.714286	0.175	0.01	3
2007-11	1.81	1.85	1.104972	4.062	4.091	2.848723	0.509	0.01	3
2007-11	2.03	2.13	2.463054	4.072	4.101	2.793834	0.519	0.02	4
2007-11	2.04	2.14	2.45098	4.672	4.73	2.5916	1.119	0.02	4
2007-11	2.55	2.65	1.960784	4.682	4.74	2.568645	1.129	0.02	5
2007-11	2.56	2.66	1.953125	5.415	5.502	2.336198	1.862	0.02	5
2007-11	2.67	2.77	1.872659	5.425	5.512	2.323718	1.872	0.02	6
2007-11	2.692	2.792	1.857355	5.902	6.008	2.256279	2.349	0.02	6
2007-11	2.899	2.999	1.724733	5.912	6.018	2.246715	2.359	0.05	7
2007-11	2.95	3.05	1.694915	6.903	7.042	2.074627	3.35	0.05	7
2007-11	3.7	3.9	2.702703	6.913	7.052	2.068452	3.36	0.02	8
2007-11	3.8	4	2.631579	8.242	8.452	2.239283	4.689	0.02	8
2007-11	4	4.2	2.5	8.252	8.462	2.234518	4.699	0.05	9
2007-11	4.1	4.3	2.439024	9.631	9.91	2.295163	6.078	0.05	9
2007-11	4.4	4.6	2.272727	9.641	9.92	2.291393	6.088	0.05	10
2007-11	4.9	5.1	2.040816	10.29	10.6	2.300727	6.737	0.05	10
2007-20	1.44	1.44		0	0				
2007-20	1.515	1.515		3.807	3.807				
2007-20	1.65	1.75		3.817	3.817		0.01	0.05	2
2007-20	1.67	1.77	2.994012	4.004	4.016	3.045685	0.197	0.05	2
2007-20	1.84	1.86	0.543478	4.014	4.026	2.898551	0.207	0.01	3
2007-20	1.845	1.865	0.542005	4.154	4.168	2.017291	0.347	0.01	3
2007-20	1.93	1.97	1.036269	4.164	4.178	1.960784	0.357	0.02	4
2007-20	1.98	2.02	1.010101	4.426	4.445	1.534733	0.619	0.02	4
2007-20	2.15	2.19	0.930233	4.436	4.455	1.510334	0.629	0.02	5
2007-20	2.18	2.22	0.917431	4.644	4.668	1.433692	0.837	0.02	5
2007-20	2.18	2.24	1.376147	4.654	4.678	1.416765	0.847	0.03	6
2007-20	2.22	2.28	1.351351	4.937	4.969	1.415929	1.13	0.03	6
2007-20	2.38	2.52	2.941176	4.947	4.979	1.403509	1.14	0.07	7
2007-20	2.48	2.62	2.822581	5.303	5.356	1.77139	1.496	0.07	7
2007-20	2.94	3	1.020408	5.313	5.366	1.759628	1.506	0.03	8

2007-20	3.04	3.1	0.986842	5.753	5.815	1.593011	1.946	0.03	8
2007-20	3.12	3.18	0.961538	5.763	5.825	1.584867	1.956	0.03	9
2007-20	3.22	3.28	0.931677	6.582	6.659	1.387387	2.775	0.03	9
2007-20	3.55	3.65	1.408451	6.592	6.669	1.382406	2.785	0.05	10
2007-20	3.6	3.7	1.388889	7.135	7.228	1.397236	3.328	0.05	10
2007-20	3.84	3.96	1.5625	7.145	7.238	1.39305	3.338	0.06	11
2007-20	4.14	4.26	1.449275	8.701	8.841	1.430323	4.894	0.06	11
2007-20	4.3	4.5	2.325581	8.711	8.851	1.427406	4.904	0.1	12
2007-20	4.5	4.7	2.222222	9.88	10.071	1.572534	6.073	0.1	12
2008-01	1.44	1.44		0	0				
2008-01	1.513	1.513		3.505	3.505				
2008-01	1.548	1.748	6.459948	3.515	3.515		0.01	0.1	2
2008-01	1.6	1.8	6.25	3.641	3.659	6.617647	0.136	0.1	2
2008-01	1.84	1.86	0.543478	3.651	3.669	6.164384	0.146	0.01	3
2008-01	1.85	1.87	0.540541	3.781	3.8	3.442029	0.276	0.01	3
2008-01	1.984	2.024	1.008065	3.791	3.81	3.321678	0.286	0.02	4
2008-01	2.01	2.05	0.995025	3.88	3.901	2.8	0.375	0.02	4
2008-01	2.03	2.07	0.985222	3.89	3.911	2.727273	0.385	0.02	5
2008-01	2.06	2.1	0.970874	4.134	4.16	2.066773	0.629	0.02	5
2008-01	2.1	2.14	0.952381	4.144	4.17	2.034429	0.639	0.02	6
2008-01	2.13	2.17	0.938967	4.471	4.503	1.656315	0.966	0.02	6
2008-01	2.15	2.25	2.325581	4.481	4.513	1.639344	0.976	0.05	7
2008-01	2.25	2.35	2.222222	4.699	4.743	1.842546	1.194	0.05	7
2008-01	2.56	2.6	0.78125	4.709	4.753	1.827243	1.204	0.02	8
2008-01	2.58	2.62	0.775194	5.373	5.427	1.445396	1.868	0.02	8
2008-01	2.65	2.75	1.886792	5.383	5.437	1.4377	1.878	0.05	9
2008-01	2.95	3.05	1.694915	7.071	7.185	1.59843	3.566	0.05	9
2008-01	3.8	3.9	1.315789	7.081	7.195	1.59396	3.576	0.05	10
2008-01	3.85	3.95	1.298701	8.342	8.49	1.529874	4.837	0.05	10
2008-01	4	4.2	2.5	8.352	8.5	1.526718	4.847	0.1	11
2008-01	4.1	4.3	2.439024	9.319	9.514	1.676987	5.814	0.1	11
2008-01	4.3	4.5	2.325581	9.329	9.524	1.674107	5.824	0.1	12
2008-01	4.4	4.6	2.272727	10.703	10.961	1.792164	7.198	0.1	12
2008-19	1.434	1.434		0	0				
2008-19	1.528	1.528		3.789	3.789				
2008-19	1.8	1.6	5.555556	3.799	3.799		0.01	0.1	2
2008-19	1.83	1.63	5.464481	3.854	3.847	5.384615	0.065	0.1	2
2008-19	1.79	1.71	2.234637	3.864	3.857	4.666667	0.075	0.04	3
2008-19	1.81	1.73	2.209945	4.044	4.029	2.941176	0.255	0.04	3
2008-19	1.96	1.84	3.061224	4.054	4.039	2.830189	0.265	0.06	4
2008-19	1.97	1.85	3.045685	4.116	4.096	3.058104	0.327	0.06	4
2008-19	2.233	2.073	3.582624	4.126	4.106	2.967359	0.337	0.08	5
2008-19	2.26	2.1	3.539823	4.513	4.464	3.383978	0.724	0.08	5
2008-19	2.583	2.423	3.097174	4.523	4.474	3.337875	0.734	0.08	6
2008-19	2.61	2.45	3.065134	4.79	4.724	3.296703	1.001	0.08	6
2008-19	4.1	3.9	2.439024	4.8	4.734	3.264095	1.011	0.1	7
2008-19	4.2	4	2.380952	5.573	5.471	2.858744	1.784	0.1	7
2008-30	1.44	1.44		0	0				
2008-30	1.514	1.514		3.787	3.787				
2008-30	1.55	1.75		3.797	3.797		0.01	0.1	2
2008-30	1.6	1.8	6.25	3.962	3.985	6.571429	0.175	0.1	2
2008-30	1.765	1.845	2.266289	3.972	3.995	6.216216	0.185	0.04	3

2008-30	1.77	1.85	2.259887	4.283	4.32	3.729839	0.496	0.04	3
2008-30	1.99	2.03	1.005025	4.293	4.33	3.656126	0.506	0.02	4
2008-30	1.995	2.035	1.002506	4.458	4.499	3.055142	0.671	0.02	4
2008-30	2.15	2.19	0.930233	4.468	4.509	3.010279	0.681	0.02	5
2008-30	2.155	2.195	0.928074	4.587	4.629	2.625	0.8	0.02	5
2008-30	2.37	2.43	1.265823	4.597	4.639	2.592593	0.81	0.03	6
2008-30	2.38	2.44	1.260504	4.867	4.917	2.314815	1.08	0.03	6
2008-30	2.428	2.627	4.098023	4.877	4.927	2.293578	1.09	0.1	7
2008-30	2.55	2.75	3.921569	5.252	5.333	2.764505	1.465	0.1	7
2008-30	2.75	2.81	1.090909	5.262	5.343	2.745763	1.475	0.03	8
2008-30	2.77	2.83	1.083032	5.438	5.522	2.543913	1.651	0.03	8
2008-30	3.052	3.152	1.63827	5.448	5.532	2.528597	1.661	0.05	9
2008-30	3.09	3.19	1.618123	5.967	6.069	2.33945	2.18	0.05	9
2008-30	3.6	3.8	2.777778	5.977	6.079	2.328767	2.19	0.1	10
2008-30	3.65	3.85	2.739726	6.283	6.402	2.383814	2.496	0.1	10
2008-30	4.2	4.6	4.761905	6.293	6.412	2.374302	2.506	0.2	11
2008-30	4.3	4.7	4.651163	7.012	7.199	2.899225	3.225	0.2	11
2009-01-4	1.44	1.44		0	0				
2009-01-4	1.514	1.514		3.827	3.827				
2009-01-4	1.55	1.75	6.451613	3.837	3.837		0.01	0.1	2
2009-01-4	1.64	1.84	6.097561	3.987	4.007	6.25	0.16	0.1	2
2009-01-4	1.7	1.9	5.882353	3.997	4.017	5.882353	0.17	0.1	3
2009-01-4	1.8	2	5.555556	4.323	4.381	5.846774	0.496	0.1	3
2009-01-4	2.03	2.07	0.985222	4.333	4.391	5.731225	0.506	0.02	4
2009-01-4	2.08	2.12	0.961538	4.65	4.715	3.948967	0.823	0.02	4
2009-01-4	2.21	2.29	1.809955	4.66	4.725	3.901561	0.833	0.04	5
2009-01-4	2.26	2.34	1.769912	4.904	4.978	3.435469	1.077	0.04	5
2009-01-4	2.78	2.82	0.719424	4.914	4.988	3.403864	1.087	0.02	6
2009-01-4	2.83	2.87	0.706714	5.575	5.659	2.402746	1.748	0.02	6
2009-01-4	3.03	3.07	0.660066	5.585	5.669	2.389078	1.758	0.02	7
2009-01-4	3.05	3.09	0.655738	6.251	6.343	1.89769	2.424	0.02	7
2009-01-4	3.45	3.49	0.57971	6.261	6.353	1.889893	2.434	0.02	8
2009-01-4	3.46	3.5	0.578035	6.556	6.652	1.758886	2.729	0.02	8
2009-02-1	1.44	1.44		0	0				
2009-02-1	1.515	1.515		3.784	3.784				
2009-02-1	1.6	1.7		3.794	3.794				
2009-02-1	1.65	1.75	3.030303	4	4.013	3.009259	0.216	0.05	2
2009-02-1	1.76	1.78	0.568182	4.01	4.023	2.876106	0.226	0.05	2
2009-02-1	1.765	1.785	0.566572	4.108	4.123	2.314815	0.324	0.01	3
2009-02-1	1.81	1.83	0.552486	4.118	4.133	2.245509	0.334	0.01	3
2009-02-1	1.815	1.835	0.550964	4.194	4.21	1.95122	0.41	0.01	4
2009-02-1	2.01	2.05	0.995025	4.204	4.22	1.904762	0.42	0.01	4
2009-02-1	2.03	2.07	0.985222	4.362	4.381	1.643599	0.578	0.02	5
2009-02-1	2.25	2.35	2.222222	4.372	4.391	1.615646	0.588	0.02	5
2009-02-1	2.28	2.38	2.192982	4.644	4.675	1.802326	0.86	0.05	6
2009-02-1	2.335	2.375	0.856531	4.654	4.685	1.781609	0.87	0.05	6
2009-02-1	2.34	2.38	0.854701	5.036	5.074	1.517572	1.252	0.02	7
2009-02-1	2.65	2.69	0.754717	5.046	5.084	1.505547	1.262	0.02	7
2009-02-1	2.68	2.72	0.746269	5.348	5.39	1.342711	1.564	0.02	8
2009-02-1	2.85	2.89	0.701754	5.358	5.4	1.33418	1.574	0.02	8
2009-02-1	2.87	2.91	0.696864	5.627	5.673	1.247965	1.843	0.02	9
2010-06	1.44	1.44		0	0				

2010-06	1.51	1.51		3.692	3.692				
2010-06	1.6	1.8	6.25	3.702	3.702		0.01	0.1	2
2010-06	1.7	1.9	5.882353	3.918	3.945	6.25	0.216	0.1	2
2010-06	1.83	1.85	0.546448	3.928	3.955	5.973451	0.226	0.01	3
2010-06	1.85	1.87	0.540541	4.174	4.205	3.283898	0.472	0.01	3
2010-06	2.1	2.14	0.952381	4.184	4.215	3.215768	0.482	0.02	4
2010-06	2.11	2.15	0.947867	4.939	4.984	1.818917	1.237	0.02	4
2010-06	2.68	2.72	0.746269	4.949	4.994	1.80433	1.247	0.02	5
2010-06	2.73	2.77	0.732601	5.772	5.829	1.376812	2.07	0.02	5
2010-06	2.82	2.88	1.06383	5.782	5.839	1.370192	2.08	0.03	6
2010-06	2.97	3.03	1.010101	6.455	6.526	1.289502	2.753	0.03	6
2010-06	3.55	3.65	1.408451	6.465	6.536	1.284835	2.763	0.05	7
2010-06	3.6	3.7	1.388889	6.793	6.874	1.310256	3.091	0.05	7
2010-06	3.67	3.73	0.817439	6.803	6.884	1.30603	3.101	0.03	8
2010-06	3.92	3.98	0.765306	8.444	8.552	1.13876	4.742	0.03	8
2010-06	4.4	4.6	2.272727	8.454	8.562	1.136364	4.752	0.1	9
2010-06	4.6	4.8	2.173913	11.28	11.514	1.543943	7.578	0.1	9
2010-21	1.44	1.44		0	0				
2010-21	1.51	1.51		3.614	3.614				
2010-21	1.65	1.75		3.624	3.624		0.01	0.05	2
2010-21	1.7	1.8	2.941176	3.884	3.9	2.962963	0.27	0.05	2
2010-21	1.85	1.89	1.081081	3.894	3.91	2.857143	0.28	0.02	3
2010-21	1.88	1.92	1.06383	4.108	4.129	2.125506	0.494	0.02	3
2010-21	2.04	2.08	0.980392	4.118	4.139	2.083333	0.504	0.02	4
2010-21	2.05	2.09	0.97561	5.021	5.059	1.350391	1.407	0.02	4
2010-21	2.83	2.87	0.706714	5.031	5.069	1.340861	1.417	0.02	5
2010-21	2.84	2.88	0.704225	6.062	6.116	1.102941	2.448	0.02	5
2010-21	3.1	3.2	1.612903	6.072	6.126	1.098454	2.458	0.05	6
2010-21	3.13	3.23	1.597444	7.062	7.147	1.232599	3.448	0.05	6
2010-21	3.56	3.64	1.123596	7.072	7.157	1.229034	3.458	0.04	7
2010-21	3.61	3.69	1.108033	8.916	9.043	1.197661	5.302	0.04	7
2010-21	3.65	3.75	1.369863	8.926	9.053	1.195407	5.312	0.05	8
2010-21	3.7	3.8	1.351351	10.271	10.435	1.231786	6.657	0.05	8
2010-21	4.6	4.8	2.173913	10.281	10.445	1.229939	6.667	0.1	9
2010-21	4.65	4.85	2.150538	11.356	11.57	1.382072	7.742	0.1	9
2011-01	1.441	1.441		0	0				
2011-01	1.444	1.444		0.479	0.479				
2011-01	1.51	1.49	0.662252	0.489	0.489		0.01	0.01	2
2011-01	1.513	1.493	0.660939	0.618	0.616	0.719424	0.139	0.01	2
2011-01	1.67	1.65	0.598802	0.628	0.626	0.671141	0.149	0.01	3
2011-01	1.671	1.651	0.598444	0.7	0.697	0.678733	0.221	0.01	3
2011-01	1.74	1.72	0.574713	0.71	0.707	0.649351	0.231	0.01	4
2011-01	1.741	1.721	0.574383	0.74	0.737	0.574713	0.261	0.01	4
2011-01	1.83	1.81	0.546448	0.75	0.747	0.553506	0.271	0.01	5
2011-01	1.831	1.811	0.54615	0.843	0.839	0.549451	0.364	0.01	5
2011-01	4.61	4.59	0.21692	0.853	0.849	0.534759	0.374	0.01	6
2011-02	1.44	1.44		0	0				
2011-02	1.5	1.5		2.235	2.235				
2011-02	1.68	1.78		2.245	2.245		0.01	0.05	2
2011-02	1.7	1.8	2.941176	2.498	2.513	2.851711	0.263	0.05	2
2011-02	1.84	1.9	1.630435	2.508	2.523	2.747253	0.273	0.03	3
2011-02	1.85	1.91	1.621622	2.607	2.627	2.688172	0.372	0.03	3

2011-02	1.9	2.1	5.263158	2.617	2.637	2.617801	0.382	0.1	4
2011-02	1.91	2.11	5.235602	2.688	2.717	3.200883	0.453	0.1	4
2011-02	2.2	2.4	4.545455	2.698	2.727	3.131749	0.463	0.1	5
2011-02	2.22	2.42	4.504505	2.862	2.908	3.668262	0.627	0.1	5
2011-02	2.85	3.05	3.508772	2.872	2.918	3.610675	0.637	0.1	6
2011-02	3	3.2	3.333333	3.075	3.137	3.690476	0.84	0.1	6
2011-02	4.3	4.5	2.325581	3.085	3.147	3.647059	0.85	0.1	7
2011-02	4.4	4.6	2.272727	4.426	4.546	2.738476	2.191	0.1	7
2011-04	1.44	1.44		0	0				
2011-04	1.505	1.505		3.397	3.397				
2011-04	1.55	1.65		3.407	3.407		0.01	0.05	2
2011-04	1.58	1.68	3.164557	3.586	3.599	3.439153	0.189	0.05	2
2011-04	1.6	1.7	3.125	3.596	3.609	3.266332	0.199	0.05	3
2011-04	1.65	1.75	3.030303	3.712	3.732	3.174603	0.315	0.05	3
2011-04	1.8	1.9	2.777778	3.722	3.742	3.076923	0.325	0.05	4
2011-04	1.82	1.92	2.747253	3.846	3.874	3.11804	0.449	0.05	4
2011-04	1.85	1.95	2.702703	3.856	3.884	3.050109	0.459	0.05	5
2011-04	1.88	1.98	2.659574	3.932	3.965	3.084112	0.535	0.05	5
2011-04	3.29	3.69	6.079027	3.942	3.975	3.027523	0.545	0.2	6
2011-04	3.31	3.71	6.042296	4.251	4.322	4.156909	0.854	0.2	6
2011-04	4.2	4.6	4.761905	4.261	4.332	4.108796	0.864	0.2	7
2011-04	4.3	4.7	4.651163	5.375	5.548	4.373104	1.978	0.2	7
2011-08	1.44	1.44		0	0				
2011-08	1.485	1.485		2.416	2.416				
2011-08	1.5	1.6		2.426	2.426		0.01	0.05	2
2011-08	1.55	1.65	3.225806	2.529	2.536	3.097345	0.113	0.05	2
2011-08	1.635	1.675	1.223242	2.539	2.546	2.845528	0.123	0.02	3
2011-08	1.637	1.677	1.221747	2.621	2.631	2.439024	0.205	0.02	3
2011-08	1.67	1.77	2.994012	2.631	2.641	2.325581	0.215	0.05	4
2011-08	1.83	1.93	2.73224	2.826	2.847	2.560976	0.41	0.05	4
2011-08	1.95	2.05	2.564103	2.836	2.857	2.5	0.42	0.05	5
2011-08	2.05	2.15	2.439024	3.019	3.05	2.570481	0.603	0.05	5
2011-08	2.7	2.9	3.703704	3.029	3.06	2.528548	0.613	0.1	6
2011-08	2.8	3	3.571429	3.836	3.925	3.133803	1.42	0.1	6
2011-08	4.2	4.6	4.761905	3.846	3.935	3.111888	1.43	0.2	7
2011-21	1.44	1.44		0	0				
2011-21	1.505	1.505		2.152	2.151				
2011-21	1.55	1.75	6.451613	2.162	2.161	5	0.01	0.1	2
2011-21	1.7	1.9	5.882353	2.34	2.363	6.117021	0.188	0.1	2
2011-21	2.1	2.2	2.380952	2.35	2.373	5.808081	0.198	0.05	3
2011-21	2.13	2.23	2.347418	2.521	2.551	4.065041	0.369	0.05	3
2011-21	2.402	2.602	4.163197	2.531	2.561	3.957784	0.379	0.1	4
2011-21	2.5	2.7	4	3.004	3.064	3.521127	0.852	0.1	4
2011-21	2.932	3.032	1.705321	3.014	3.074	3.480278	0.862	0.05	5
2011-21	2.96	3.06	1.689189	4.052	4.138	2.263158	1.9	0.05	5
2011-21	3.952	4.052	1.265182	4.062	4.148	2.251309	1.91	0.05	6
2011-21	4.05	4.15	1.234568	4.727	4.899	3.339806	2.575	0.05	6

Appendix 4: Source Calibration and Sound Dissipation Results

This appendix describes the technology and measurements that were used to record the source signature and dissipation of the airgun system during the 2010 and 2009 field programs respectively.

During both experiments, a square wave trigger signal was supplied to the firing system hardware by a FEI-Zyfer GPStarplus Clock model 565, based on GPS time. Gun firing and synchronization was controlled by a RealTime Systems LongShot fire controller, which sent a voltage to the gun solenoid to trigger firing. There was an approximate 54.8 ms delay between trigger and fire point.

Pressurized air for the pneumatic G-guns was supplied by two Hurricane compressors, model 6T-276-44SB/2500. These are air cooled, containerized compressor systems. Each compressor was powered by a C13 Caterpillar engine which turns a rotary screw first stage compressor and a three stage piston compressor capable of developing a total air volume of 600 SCFM @ 2500 PSI. The seismic system was operated at 1950 PSI and one compressor could easily supply sufficient volume of air under appropriate pressure.

Seismic Source Levels: calibration

Seismic Calibration experiments were conducted in 2009 and 2010, including source level calibration and dissipation measurement. While these results are most relevant to signal processing for the multichannel seismic reflection data, they are presented here as the background for understanding sources levels and propagation in the water column, which was utilized in determining sonobuoy offsets from the direct water wave arrival.

Julian Day 222
Ship Position: 71.3058º -136.9920º

Equipment
Hydrophone: NRCan #22;
Calibration (June 11, 2010), -200.3 dB//V/uPa (low gain) on SCU #6
GSCDig #4 Channel 1
0.9794 = calibration factor of GSCDig 4 Ch 1 (June 11, 2010)
SCU-6 s/n 025
Realtime Systems LongShot firing system

Results from the 2010 calibration are summarized in the tables and figures below.

Table 4-1: Calibration results, 0 to peak amplitude

Hydro-phone Depth (m)	Trace	Distance (m)	Amp (Bar)	Amp (Bar.m)	0-Peak Amp (dB)	0-Peak Amp dB re 1 μPa@1m
107	5307	106.44	0.049692425	5.289	193.93	234.5
104.2	5308	107.60	0.04803056	5.168	193.63	234.3
101.85	5309	108.11	0.04695705	5.076	193.43	234.1
98.86	5310	108.58	0.047067735	5.111	193.45	234.2
96.3	5311	109.18	0.047847748	5.224	193.60	234.4
94.2	5312	109.44	0.046665367	5.107	193.38	234.2
92	5313	109.65	0.046593013	5.109	193.37	234.2
90.2	5314	110.49	0.047146439	5.209	193.47	234.3
88.08	5315	110.72	0.045459398	5.033	193.15	234.0
86.4	5316	111.44	0.045696872	5.092	193.20	234.1
84.9	5317	111.79	0.045353476	5.070	193.13	234.1
			Average	**5.135**		**234.2**

Table 4-2: Calibration results, peak-to-peak amplitude

Hydro-phone Depth (m)	Trace	Distance (m)	Amplitude (Bar)	Amplitude (Bar.m)	Peak-Peak Amp (dB)	Peak-Peak Amp dB re 1 m
107	5307	106.44	0.090562924	9.640	199.14	239.7
104.2	5308	107.60	0.094785972	10.199	199.53	240.2
101.85	5309	108.11	0.092606064	10.011	199.33	240.0
98.86	5310	108.58	0.093101652	10.109	199.38	240.1
96.3	5311	109.18	0.095314902	10.406	199.58	240.3
94.2	5312	109.44	0.090167815	9.868	199.10	239.9
92	5313	109.65	0.093468864	10.249	199.41	240.2
90.2	5314	110.49	0.09026285	9.973	199.11	240.0
88.08	5315	110.72	0.086167498	9.541	198.71	239.6
86.4	5316	111.44	0.090268747	10.059	199.11	240.1
84.9	5317	111.79	0.088463308	9.890	198.94	239.9
			Average	**9.995**		**240.0**

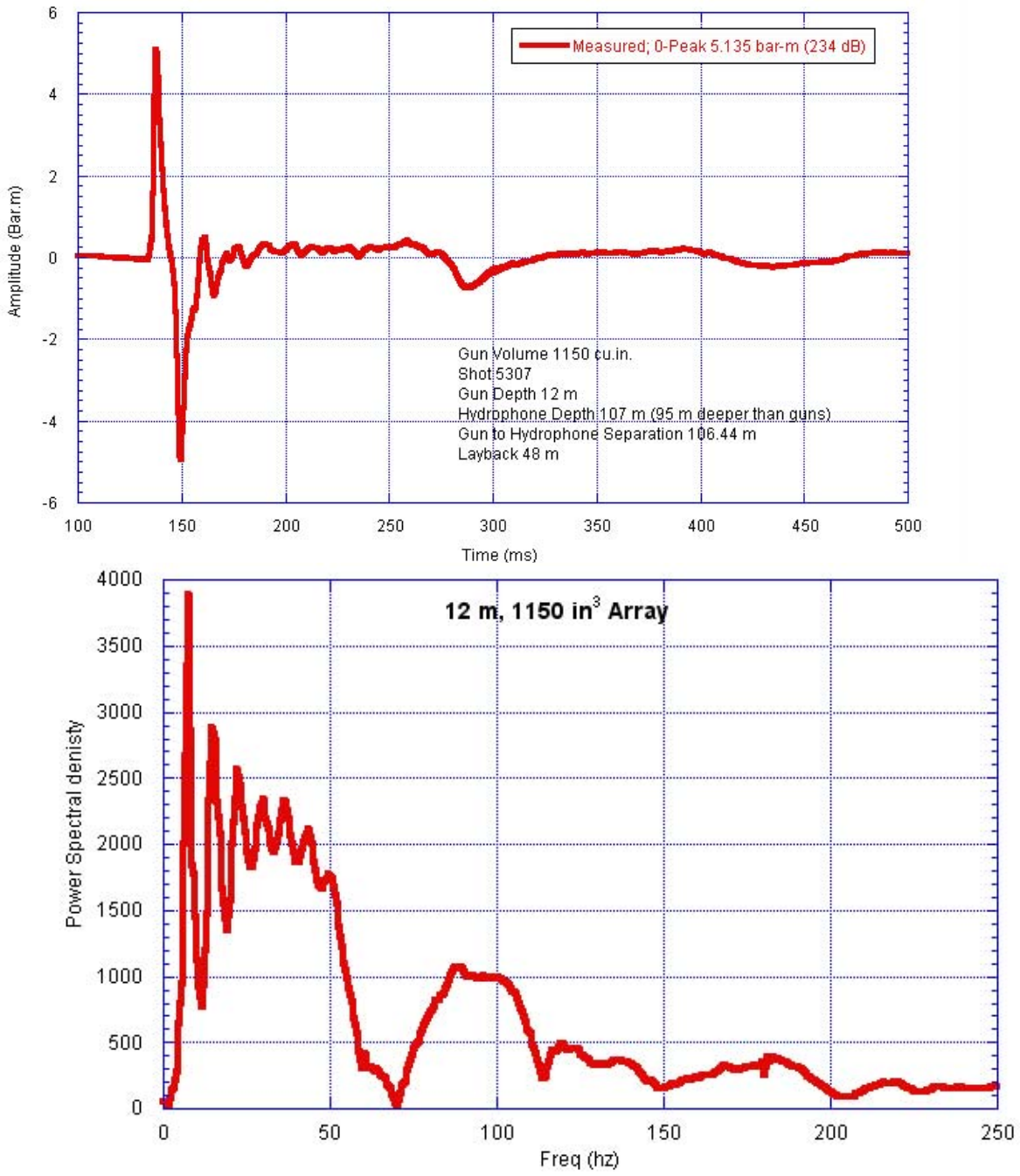

Figure 4-1. Calibration test result, shot 5307. Top is a time domain shot signature showing a zero to peak amplitude of 5.135 bar-m or 234 dB re 1 μPa at 1 m. Bottom is the frequency spectrum plot for this trace, showing prominent power between 2 and 60 Hz with notching occurring at 65 Hz, caused by the bubble pulse period.

Model

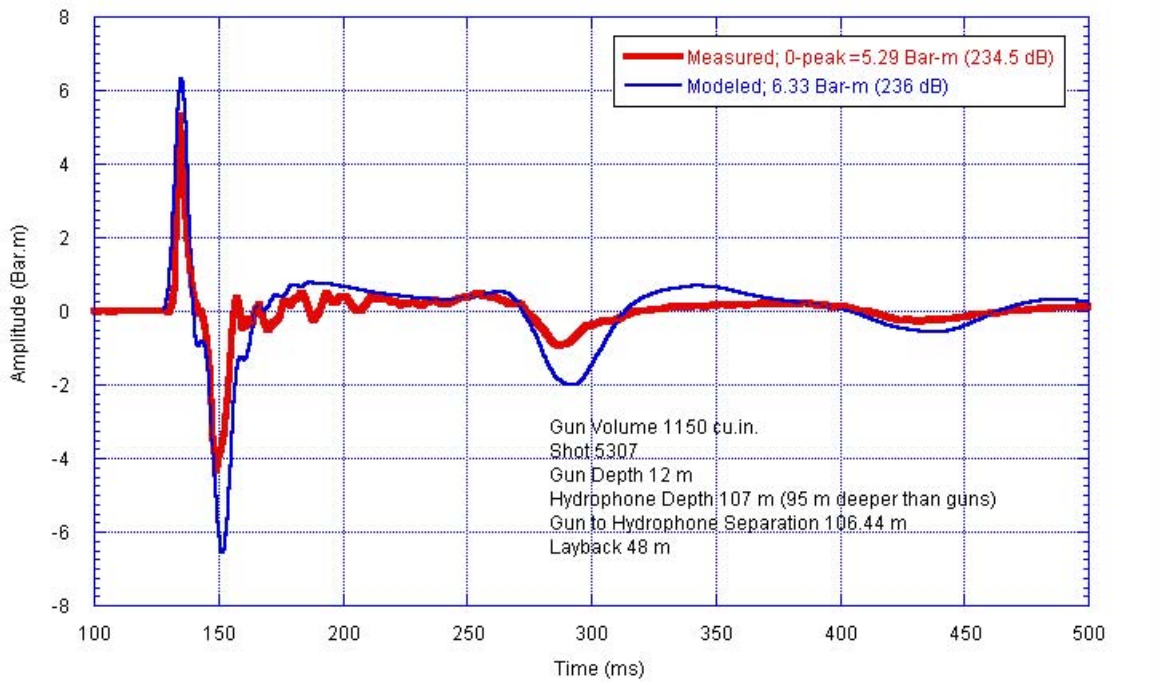

Figure 4-2. Comparison of the measured and modeled time-signature results. Note the 0-Peak amplitude of the model suggests 6.33 Bar-m (236 dB re 1 mPa @ 1 m), while the measured result is 5.29 Bar-m (234.5 dB re 1 mPa @ 1 m). This difference is consistent but unexplained.

Table 4-3: Amplitude values reported from the model compared with the field measurement (RMS was calculated for the initial positive and negative peaks of the signatures - a duration of 20 ms).

	Model/Measure Bar-m	Model/Measure MPa	Model/Measure db re 1 μPa@1m
Peak to peak in bar-m.	12.9 / 10.0	1.29 / 1.00	242 / 240.0
Zero to peak in bar-m.	6.33 / 5.29	0.633 / 0.529	236 / 234.5
RMS pressure in bar-m.	4.48 / 2.49	0.448 / 0.249	233 / 228

Seismic Source Levels: Dissipation

Seismic sound dissipation (attenuation) experiments were conducted in 2009. In this experiment, two vessels were used; one deployed the source array and the other the receiver (hydrophone). The source vessel sailed a figure-8 pattern around the receiving vessel (Figure 4-3).

Equipment

1) 1150 cu in. Seismic source array (on CCGS Louis S. St. Laurent), consisting of two 500 in^3 Sercel G-guns and one 150 in^3 G-gun

2) Two calibrated hydrophone systems for receive signals on the USCGC Healy

3) Recording hardware (GSCDig unit #4 and TEAC LX-110)

4) GPS for ship position and heading information and absolute time (recorded)

5) Two precision GPS clocks (e.g. Zyfer GPSstarplus model 565) for synchronizing triggers between source and receivers.

6) Sound velocity profiler or CTD/XCTD for providing water column sound velocity.

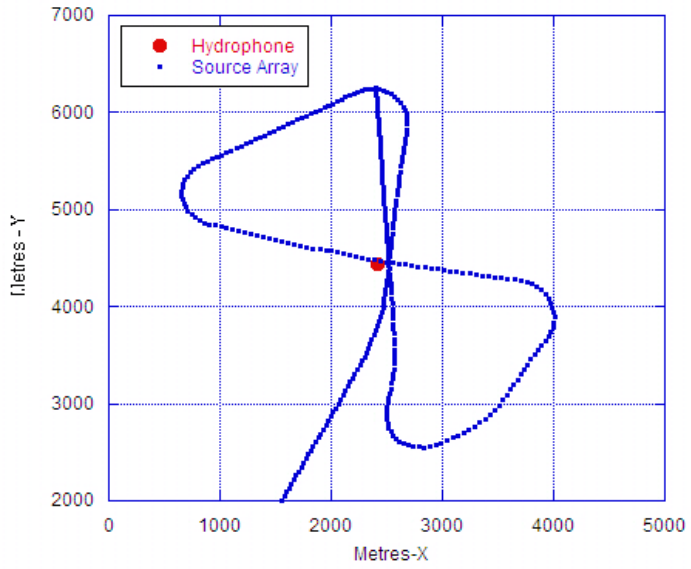

Figure 4-3. Relative positions of the hydrophone and source array during the experiment.

At the first rendezvous position for the CCGS *Louis S. St.-Laurent* (LSSL) and the USCGC *Healy* (Healy): using a two-ship operation, the sound pressure field was measured with a receiving ship (Healy) and a shooting ship (LSSL). The two independent single element calibrated hydrophones were hung vertically in the water column from the stern of the Healy as it remained relatively stationary. The LSSL towed the seismic source as it ran a pattern of variable offset from the Healy. The experiment was conducted on August 11 (Day 223), 2009, commencing at 0622Z when the two ships first rendez-voused, in open water conditions. Sea state was calm. The two hydrophones were hung from the stern of the HEALY, one hung at 92 m below the water line, the other 52 m below the water line. The experiment was terminated at 0824Z, Day 223.

The LSSL proceeded to navigate a figure-8 pattern towing the source array, following Society of Exploration Geophysicists (SEG) standard procedures (Johnston et al., 1988). The HEALY remained relatively stationary (allowed to drift) at the center of the figure-8 pattern. Ship position and heading information was recorded as part of the navigation NMEA strings for both vessels. Received direct seismic signals were recorded by the Healy during these operations, with the GSCDig Unit 4 and the

TEAC LX110 digital recorder. The firing and record triggers were synchronized by the two Zyfer GPS clocks, set to trigger every 20 seconds on the even minute. Periodically, gain functions were changed in order to accommodate changing signal amplitudes. The following table summarizes these changes and gain corrections must be accommodated on signal analysis.

Table 4-4: Input gains on calibration units

Time (GPS)	Input Gain	Comment
062200	High	Old hydrophone to rented black scu to GSCDig 4
064100	Low	New hydrophone to GSC orange scu6 to TEAC Channel 1
064544	Low	Trigger from Zyfer clock, boosted with small Heffler amplifier.
065127	Low	TEAC Ch1 signal, Ch2 Trig, Ch3 Nav
065330	High	
073230	Low	
073511	High	
075000		Changed compact flash
082349		Systems Off

The received source signals were then analyzed for peak voltage for each shot. These voltages were converted to pressure and dB and plotted as a function of distance of separation between the source and receiver.

Results

Navigation

HEALY navigation data acquired by their POS/MV integration Differential GPS and inertial navigation system. The hydrophones were located on the stern of the vessel, 89 m aft of the POSMV broadcast position. The LSSL position is recorded as the GPS antenna position which is 89 m forward of the position of the center of the source array astern of the vessel. Geographic coordinate positions were corrected to reflection positions of the hydrophone and source array using the ships heading to correct for offset from the recorded position. The duration of the experiment was between 0620Z, Day 223 (August 11, 2009) and 0824Z, Day 223. The HEALY drifted 1266 m to the NE during the course of the experiment; however, relative position data shown in Figure 4-3 have reduced this drift to a single point and corrected the LSSL position accordingly. Distance of separation between the source array and the hydrophone is shown in Figure 4-4. The closest point of intersection of the two ships was 41 m during the second pass.

Water Structure

A full ocean depth CTD cast was accomplished immediately following the calibration experiment with a SeaBird 9 instrument. Position of the cast was 74º 50.40’ N, 156º 34.31’ W at 08:47:31Z, Day 223; filename 200921-0001.cnv. Sound velocity results from this CTD show significant structure within the top 200 m (Figure 4-5). This complexity is not reflected in the density profile, although the greatest change in density occurs through this interval as well (Figure 4-7).

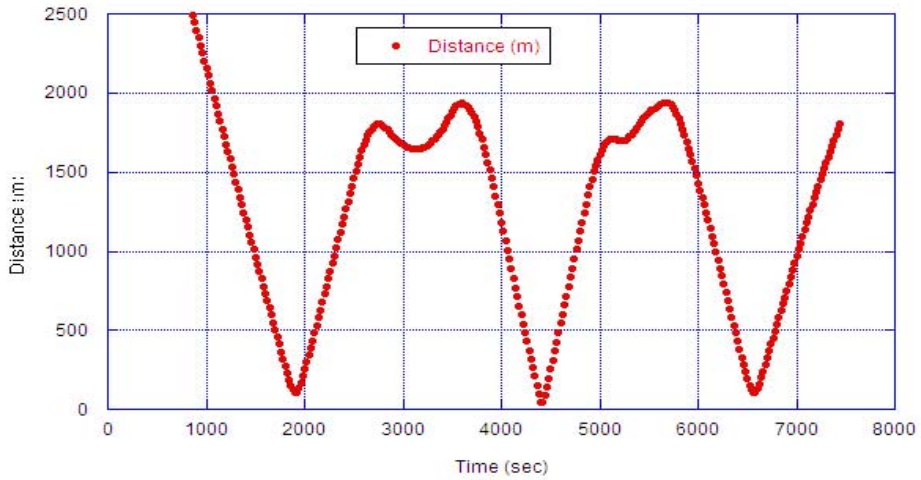

Figure 4-4. Distance of separation between the source array and receiver during the course of the experiment. X-axis is in seconds time from the start of the experiment.

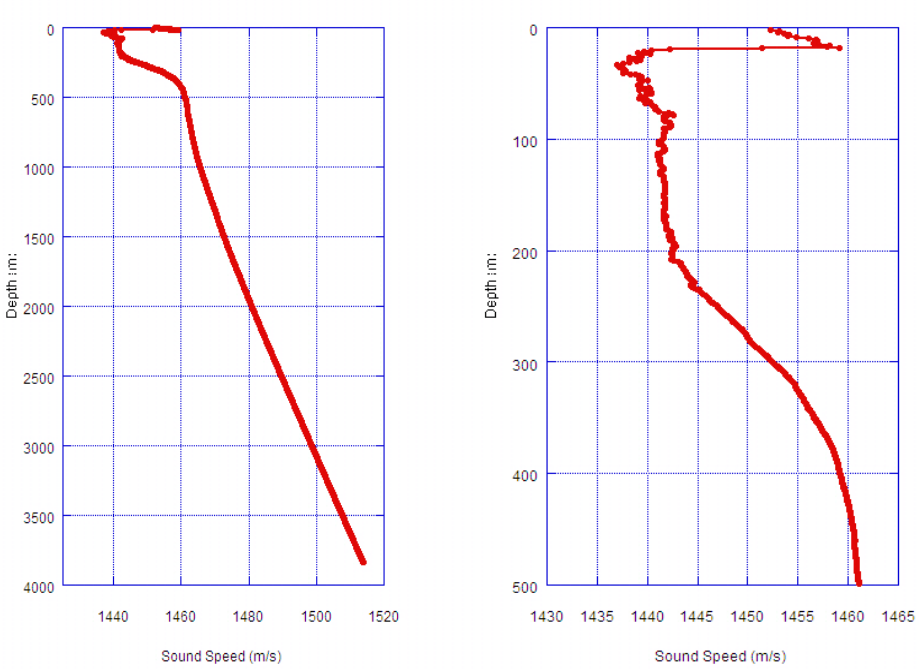

Figure 4-5. Sound velocity profile of the water column at the experiment site: to the left is the profile down to 3915 m; on the right is an enlargement of the top 500 m, showing complexity in the velocity structure, including a velocity inversion within the top 200 m.

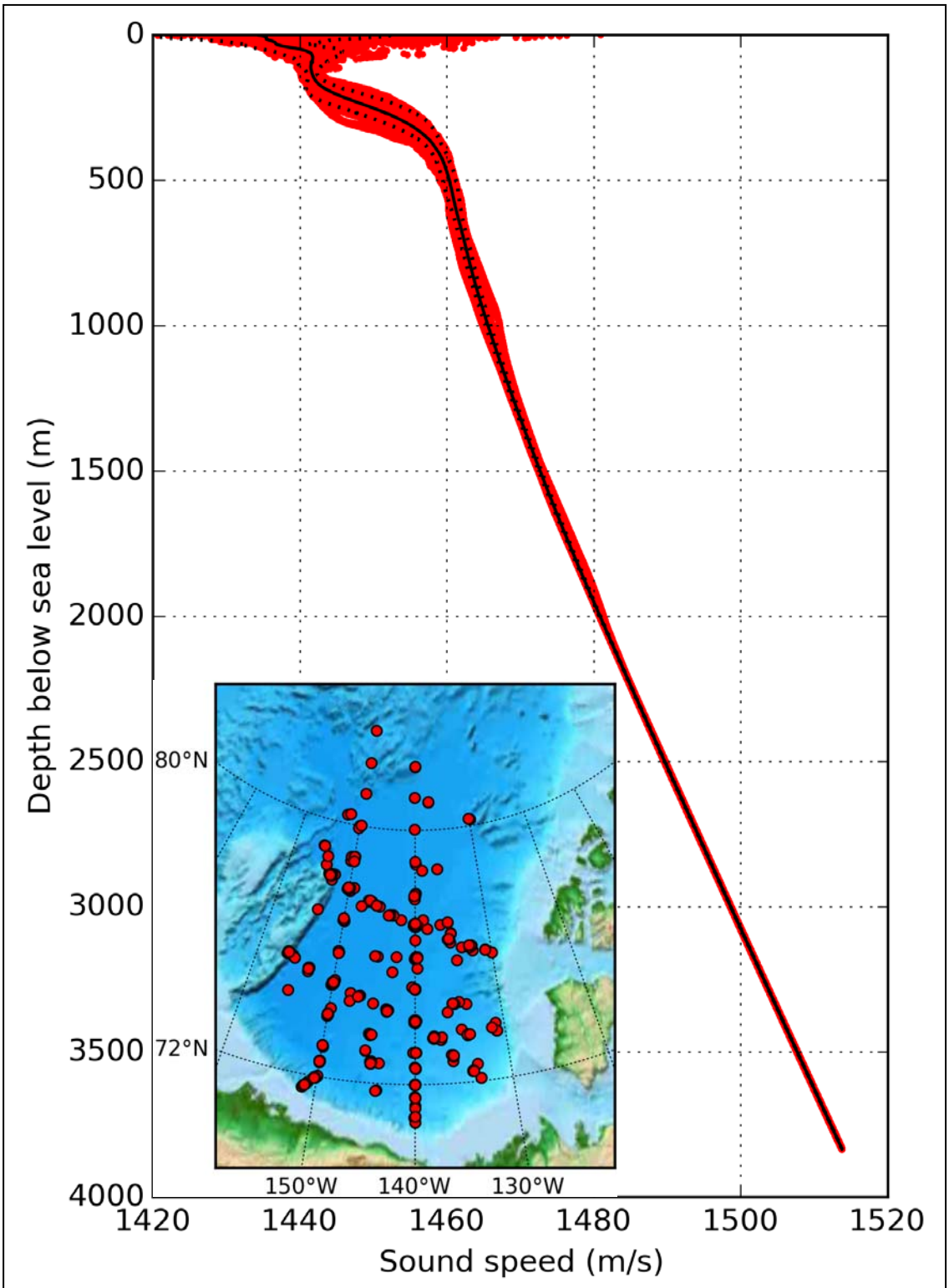

Figure 4-6. Sound velocity profile of water column compiled for 430 CTD casts (marked by red dots in the inset map) that were collected in > 1500 m of water, east of 160°W, during cruises on the Louis for all years between 2003 and 2013. The data are in courtesy of the Beaufort Gyre Project (http://www.whoi.edu/page.do?pid=66521). Mean sound speed profile (thick black line) and the mean plus and minus two standard deviations (dotted black lines). These statistics were calculated within binned depth intervals of 1 m.

Signal Amplitude

On the GSCDig digitizing system, signals are discretized by a 24-bit sigma-delta analog to digital converter and written to SEGY file format. The receiving hydrophone signal on the HEALY was brought into the SCU6 signal conditioning unit via the supplied hydrophone deck cable. The SCU6 provided power to the hydrophone and signal gain settings only; the signal was then directed to the GSCDig unit 4 via co-axial cable. Commencement of each record (trace) was initiated by a trigger from the Zyfer clock at 20 second intervals, synchronized with the Zyfer trigger clock on the LSSL. For this experiment, signals were digitized at 1 ms for a record length of 6250 ms. The recorded SEGY file was loaded into Gedco Vista 9.0 processing software to extract signal amplitudes (see Figure 4-8). In Vista, the peak maximum and peak minimum

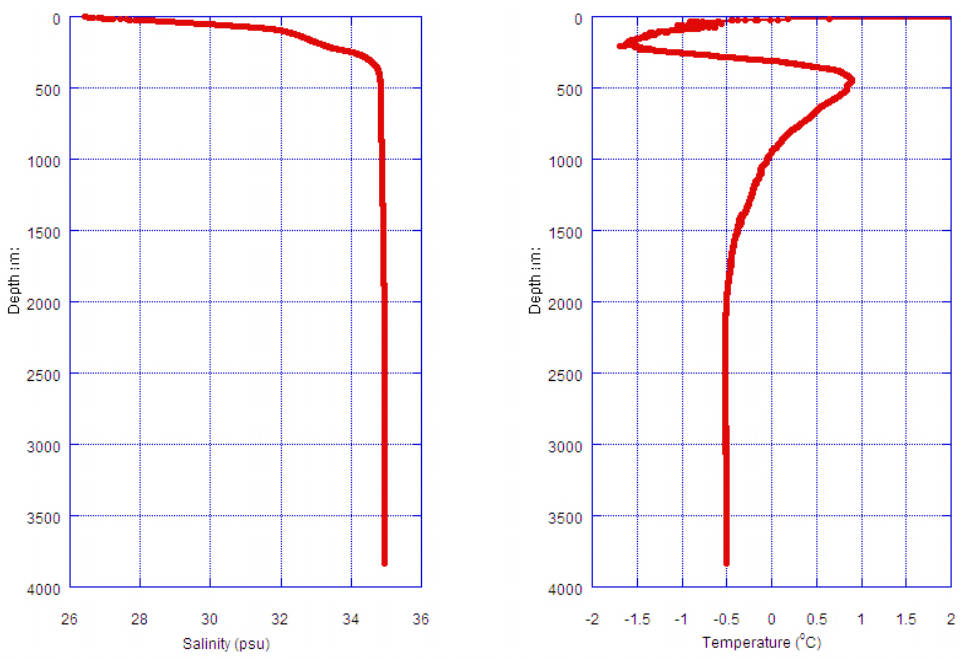

Figure 4-7. Left is the water column salinity profile; notice the greatest change in the top 500 m. Right is the temperature profile, again reflecting significant abrupt change within the top few hundred metres, including a temperature reversal in the top 200 m.

amplitudes were extracted for the first (direct) arrival for each trace, as well as the travel time (time of flight) of that first break. The travel time, using water velocity, can be converted to distance to cross check the distance recorded from navigation data.

Amplitudes in the SEGY file from the GSCDig are given in counts; a proxy for voltage. The GSCDig samples are 24 bit over a range of ± 18V. Each count, therefore, represents 2.146×10^{-6}V and allows total counts to be converted to volts.

e.g. convert a 250 mV to dB//1Volt; $20 \log_{10}(0.25/1)$ = -12.04 dB//1V
pressure at hydrophone = -12.04 - -198.5 dB//1uPa = 186 dB//1uPa. The volts have cancelled.

In terms of acoustic units; the decibel, $dB=20\log(p_1/p_2)$ where p is pressure, p_1 being the voltage measured and p_2 a reference level, which is 1 Volt. The result is in the units of dB//V, therefore. Since we are working against the signal flow, i.e., voltage to pressure

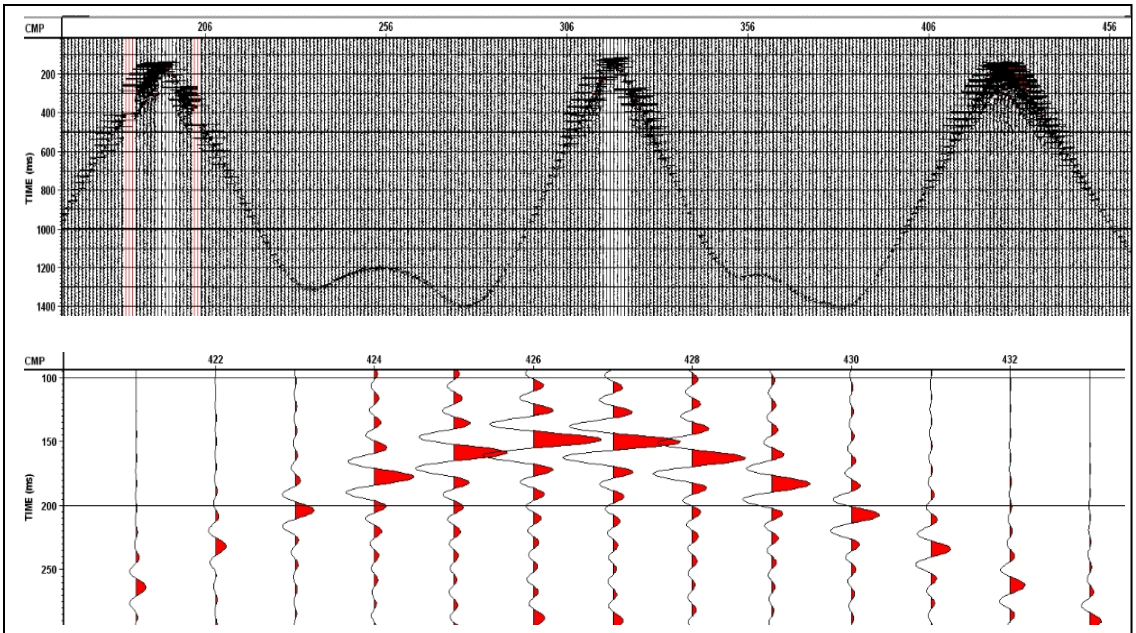

Figure 4-8. Received signals on GSCDig, displayed as wiggle traces; the amplitude of the wavelet representing received signal strength. Top panel shows all three passes of the LSSL by the HEALY; bottom panel is an enlargement of the last pass, showing increasing amplitude as the source comes closer to the proximity of the receiver. With each pass, travel time to the arrival decreases and amplitude increases.

then we negate the sensitivity value to get the pressure. The sensitivity of the calibrated hydrophone is removed from this result, providing signal level in dB. The hydrophone sensitivity in the case of this experiment depends on the gain setting: high gain: -179.1 and low gain setting: 198.5 dB//1V μPa.

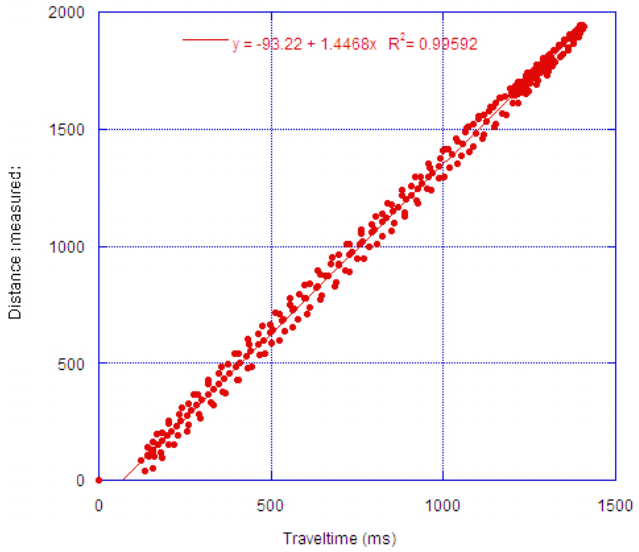

Figure 4-9. Regression of distance measured against traveltime, provided a slope (sound velocity) of 1447 m/s).

Maximum amplitudes for each trace were prepared in this way and separation distance of source and receiver was calculated in two ways; 1) traveltime from shot to receiver, based on an average sound velocity of 1440 m/s in the upper 200 m of the water column (see Figure 4-5), and by the measured distances from GPS positioning (see Figure 4-4). Regressing time of flight with distance measured results in a velocity of 1447 m/s with an r^2 value of 0.99 (Figure 4-9).

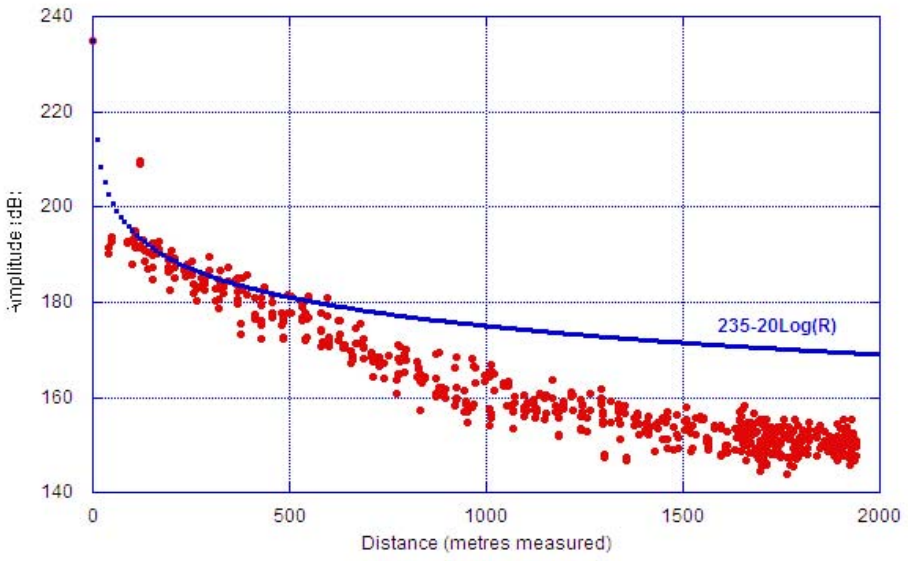

Figure 4-10A. Peak amplitude (in dB) of seismic traces (both peak positive and peak negative) compared with a 20LogR geometrical spreading loss curve. Separation distance is plotted based on signal travel time and a sound velocity of 1440 m/s.

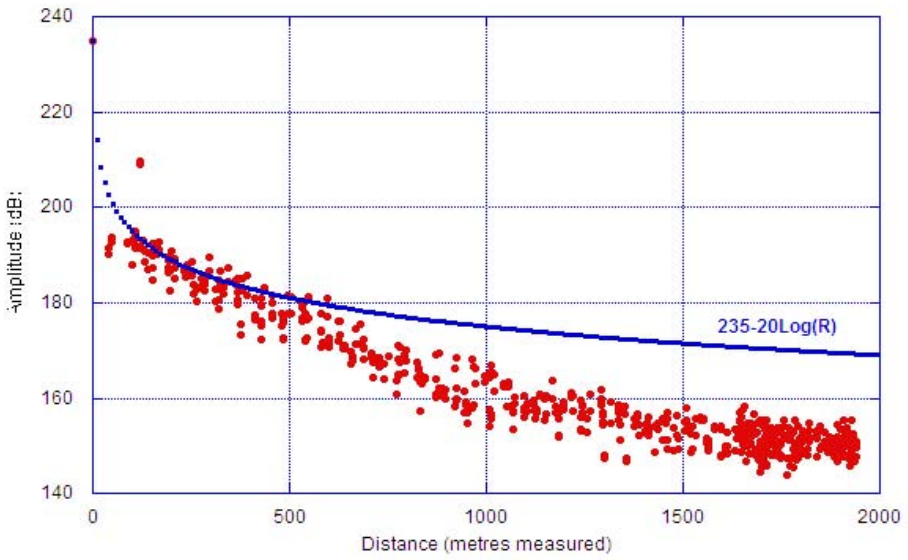

Figure 4-10B Peak amplitude (in dB) of seismic traces (both peak positive and peak negative) compared with a 20LogR geometrical spreading loss curve. Separation distance is plotted based on measured separation from GPS navigation data.

Discussion of results

Figures 4-10A and B shows the dissipation of sound as measured compared with a 20LogR curve, which is the predicted dissipation of sound along an expanding sphere, assuming conservation of energy. In general, there is a good fit between the measured and expected curves within the first 500 m; particularly for the measured distance curve (Figure 4-10B). These results show the 180 dB level is reached at a 500 m radius, assuming an initial peak pressure of 235 dB re 1 μPa at 1 m (see section above). Separation of the curves occurs at about this point. An explanation for this difference is not known but it is hypothesized that the low sound speed velocity layer in the top 200 m of the water column (as shown in Figure 4-5 and Figure 4-6) may introduce complexities in the sound propagation path. In particular, the high velocity surface layer of the top 20 m over a low velocity layer may have led to downward refraction of sound. This effect would be more apparent at further distances of separation between source and receiver.

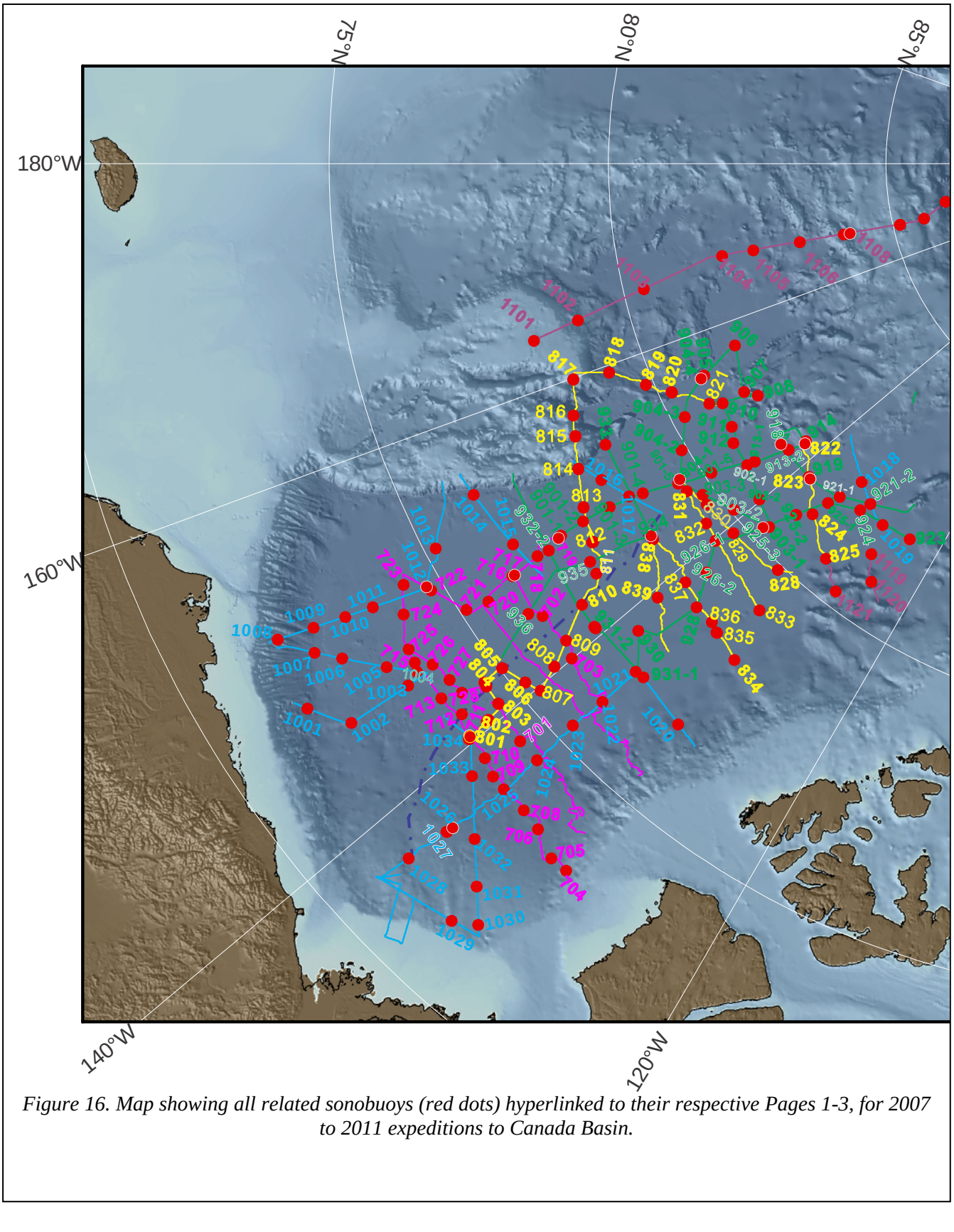

Figure 16. Map showing all related sonobuoys (red dots) hyperlinked to their respective Pages 1-3, for 2007 to 2011 expeditions to Canada Basin.